

1 Classification of Large-Scale Environments that drive the formation
2 of Mesoscale Convective Systems over Southern West Africa

3
4 Francis Nkrumah^{1,2}, Cornelia Klein^{3,5}, Kwesi Akumenyi Quagraine^{1,4}, Rebecca Berkoh
5 Oforiwaa^{2,6}, Nana Ama Browne Klutse^{2,6}, Patrick Essien^{1,2}, Gandomè Mayeul Leger Davy
6 Quenum^{2,7} and Hubert Azoda Koffi⁶

7
8 ¹Department of Physics, University of Cape Coast, Private Mail Bag, Cape Coast, Ghana;

9 ²African Institute of Mathematical Sciences (AIMS), Sector Remera, Kigali 20093, Rwanda;

10 ³U.K. Centre for Ecology and Hydrology, Wallingford, United Kingdom

11 ⁴Climate System Analysis Group (CSAG), ENGEO, University of Cape Town, Private Bag X3, Rondebosch,
12 Cape Town 7701, South Africa

13 ⁵Department of Atmospheric and Cryospheric Sciences, University of Innsbruck, Innsbruck, Austria

14 ⁶Department of Physics, University of Ghana, Legon P.O. Box LG 63, Ghana

15 ⁷National Institute of Water (NIW), University of Abomey-Calavi, Godomey, Cotonou 01 PB: 4521, Benin

16
17 *Correspondence to:* Francis Nkrumah (francis.nkrumah@ucc.edu.gh) and Nana Ama Browne Klutse
18 (nklutse@ug.edu.gh)
19

20 **Abstract.** Mesoscale convective systems (MCSs) are frequently observed over southern West Africa (SWA)
21 throughout most of the year. However, it has not yet been identified what variations in typical large-scale
22 environments of the West African monsoon seasonal cycle may favour MCS occurrence in this region. Here, ~~ninesix~~
23 distinct synoptic states are identified and are further associated with being either a dry ~~season, pre-, post-transition,~~
24 or ~~peak-~~monsoon ~~season~~ synoptic circulation type using self organizing maps (SOMs) with inputs from reanalysis
25 data. We identified a pronounced annual cycle of MCS numbers with frequency peaks in ~~June~~April and
26 ~~Septem~~October that can be ~~associated with peak rainfall during the major and minor rainy seasons respectively~~
27 ~~across SWA~~associated with the start of rainfall during the major rainy season and the maximum rainfall for the
28 ~~minor rainy season across SWA respectively~~. Comparing daily MCS frequencies, MCSs are most likely to develop
29 during ~~post-monsoon~~transition conditions featuring a northward-displaced moisture anomaly (~~0-422.8~~ MCSs per
30 day), which can be linked to strengthened low-level westerlies. Considering that these ~~post-monsoon~~transition
31 conditions occur predominantly ~~from September and into November~~during the pre- and post-monsoon season, these
32 patterns may in some cases be ~~representative of monsoon onset conditions or a delayed monsoon~~
33 ~~retreat~~representative of a delayed monsoon retreat. On the other hand, under-~~peak~~ monsoon conditions, we observe
34 ~~easterly wind anomalies~~weakened low-level south-westerlies during MCS days, which reduce moisture content over
35 the Sahel but introduce more moisture over the coast. Finally, we find a ~~majority of~~ MCS-day synoptic states to
36 exhibit positive zonal wind shear anomalies. Seasons with the strongest zonal wind shear anomalies are associated
37 with the strongest low-level temperature anomalies to the north of SWA, highlighting that a warmer Sahel can
38 promote MCS-favourable conditions in SWA. ~~These significant positive zonal wind shear anomalies for MCS days~~
39 ~~illustrate the importance of zonal wind shear for MCS development in SWA throughout the year. Overall, the~~
40 ~~SOMS-identified synoptic states converge towards high moisture and high shear conditions on MCS days in SWA,~~
41 ~~where the frequency at which these conditions occur depends on the synoptic state.~~

42 1 Introduction

43 The region of West Africa is subject to variability in rainfall on both spatial and temporal scales.
44 Fundamentally, the rainfall pattern in West Africa is modulated by the annual change in the position of the
45 Intertropical Convergence Zone (ITCZ) and the West African Monsoon (WAM). Due to endemic poverty, lack of
46 infrastructure and technology, rapid population increase, and significant fluctuation of the WAM, West Africa has
47 been deemed one of the world's most susceptible regions to climate change (IPCC, 2014). The climate of southern
48 West Africa (SWA) can be categorized into four seasonal stages: a dry season from December to February, two wet
49 seasons lasting from April to June, and September to November, and the so-called little dry season in August (e.g.
50 Thorncroft et al. 2011). Between March and June, when low-level winds are more westerly and the intertropical
51 convergence zone (ITCZ) starts to move northward, the precipitable water peaks over SWA (Klein et al. 2021). The
52 ITCZ retreats southward in September, creating the second rainy season, followed by a dry season from November
53 to January.

54 One major atmospheric disturbance that contributes to the WAM is the presence of Mesoscale Convective
55 Systems (MCSs) which supplies around 30-80 % of the total rainfall during the WAM (Klein et al. 2018). MCSs are

56 organized thunderstorm clusters, often defined to have a minimum horizontal extent of the precipitating area of 100
57 kilometres in at least one direction (Guo et al. (2022); Chen et al. (2022); Houze (2004)). Maranan et al. (2018) note
58 that diverse MCS sub-groups such as squall- or disturbance lines, structured convective systems, and mesoscale
59 convective complexes impact the hydro-climate of West Africa. In both the tropics and midlatitudes, MCS also
60 contributes significantly to rainfall extremes, rendering them a substantial contributor to the hydrologic cycle (Feng
61 et al. (2021); Li et al. (2020)). More studies have been motivated in recent decades by evaluating drivers that affect
62 rainfall variability and intensity associated with MCSs (Baidu et al. (2022); Augustin et al. (2022)). MCSs, for
63 instance, supply essential precipitation and, as a result, supply water to agriculturally productive regions in the
64 tropics, particularly in semi-arid regions such as the Sahel (Nesbitt et al. (2006)).

65 However, relative to our understanding of MCS drivers in the Sahel, SWA has received less attention. The
66 connections of MCSs to larger-scale atmospheric motion and states are both important and not fully understood for
67 the southern region, hence, a better understanding of large-scale MCS drivers is important for improving
68 precipitation prediction over SWA. Earlier research has suggested an increasing role of other types of less-organized
69 rainfall in place of MCSs over the Guinea Coast (e.g. (Acheampong, 1982; Fink et al., 2006; Kamara, 1986;
70 Omotosho, 1985), with MCS contribution to annual rainfall decreasing from 71% in the Soudanian to 56% in the
71 coastal zone (Maranan et al 2018), emphasizing MCS importance across the SWA region. Maranan et al., 2018 also
72 concluded that precipitable water and Convective Available Potential Energy (CAPE) determine where MCSs may
73 occur in SWA, while zonal wind shear is a stronger predictor for distinguishing between small scattered convection
74 and MCS-type development. Indeed, zonal wind shear intensification was found to be a major driver of increasing
75 frequencies of the most intense Sahelian MCSs over the last three decades (Taylor et al., 2017), a mechanism that
76 was similarly found to play a role for early-season MCS intensification in SWA (Klein et al 2021). Zonal wind
77 shear, which is thought to modulate the storm-available supply of moist buoyant air, is also seen to be very critical
78 to the organization of convective systems (e.g., Alfaro, 2017; Mohr & Thorncroft, 2006). Accordingly, propagating
79 storms with longer-lasting organized precipitation systems were consistently found to be associated with strong
80 vertical wind shear and higher values of CAPE in the Sahel (Hodges & Thorncroft, 1997; Laing et al., 2008; Mohr
81 & Thorncroft, 2006).

82 Previous studies address the large-scale settings for WAM-related rainfall throughout the seasons (Sultan
83 and Janicot, 2003) with less attention given to the importance of large-scale WAM modes and their effect on
84 regional MCS frequencies in SWA. The role of regional MCS-centred environments in the initiation and
85 development of MCSs in West Africa has been well studied (e.g., Klein et al. 2021; Vizy and Cook 2018; Schrage et
86 al. 2006; Maranan et al. 2018). Vizy and Cook (2018) observed that the extension of vertical mixing to the level of
87 free convection, as a result of surface heating, tends to initiate MCSs in an environment where the mid-tropospheric
88 African easterly wave disturbance is located in the east. The vertical wind shear is enhanced as a result of the
89 synoptic disturbance. Klein et al. (2021) suggested that heavy rainfall, due to cold MCSs during both dry and rainy
90 seasons, occurs in an environment with stronger vertical wind shear, increased low-level humidity, and drier mid-
91 levels. Unlike vertical wind shear, Maranan et al., (2018) suggested that thermodynamic conditions such as CAPE
92 and Convective Inhibition (CIN) are of lesser importance for the horizontal growth of convective systems, although

93 they indicate the potential of the initial vertical development of convective systems. Janiga and Thorncroft (2016)
94 also suggested that CAPE, vertical wind shear and column relative humidity are the decisive large-scale
95 environmental parameters that control the characteristics of convective systems. Based on radar and sounding
96 observations aligned around 15°N, Guy et al. (2011) analyzed MCSs and their respective environmental conditions
97 over three different regimes of West Africa (maritime, coastal, and continental). They concluded that MCSs tend to
98 occur ahead of the African easterly wave (AEW) trough during the maritime and the continental regime, while they
99 are mostly found behind the trough in the coastal regime.

100 It is not clear to what extent different large-scale patterns of atmospheric drivers such as temperature, wind,
101 humidity, and CAPE at different stages of the WAM drive the formation of MCSs over SWA. The SWA region
102 differs from its Sahelian counterpart in its closer proximity to the ocean and a distinct bimodal rainfall seasonality.
103 The WAM stages can broadly be classified into a dry season when north-easterly Harmattan winds prevail over most
104 of West Africa during December-February when rainfall mostly occurs off the southern coast of the continent
105 (Thorncroft et al 2011), and the monsoon season from July-September, initiated by a striking jump of the monsoonal
106 rainfall band from coastal regions to the Sahel (Hagos and Cook, 2007). The monsoon months thus represent the
107 unimodal Sahelian rainfall season. In SWA however, the majority of rainfall occurs between the dry months and
108 monsoon months, when the monsoon rainband first passes northward over southern regions from March to June, and
109 subsequently moves southward again when the monsoon retreats in October (e.g. Maranan et al 2018, Klein et al
110 2021). Here, we define these months when SWA receives most of its rainfall as transition season.

111 From this SWA perspective Hence, our this study systematically classifies the different large-scale patterns across the
112 WAM region and how they are associated with MCSs over SWA. For this purpose, a classification using a self
113 organizing map (SOM; Kohonen 2001) analysis was carried out to characterize large-scale WAM patterns during
114 the 1981-2020 period, which we subsequently grouped into days with MCS occurrence over SWA. The SOM is a
115 clustering technique that is topologically sensitive and uses an unsupervised training method to cluster the training
116 data (Lennard and Hegerl, 2014; Quagraine et al. 2019). This methodology thus allows us to identify favourable
117 types of large-scale environments driving the formation of MCSs within different WAM stages.

118 The paper is organized as follows: Section 2 details the study area and data sources and how they were
119 processed. In section 3, the SOM methodology and other needed statistics used to investigate the relationship
120 between large-scale environment patterns and particular MCSs are presented. Section 4 discusses the main results,
121 which include the common features and different types of large-scale patterns associated with MCSs. Section 5
122 provides the summarized conclusions of the study.

123 **2 Data Sources and Processes**

124 **2.1 ERA5 Reanalysis Data and MCS Data**

125 The ECMWF fifth-generation atmospheric reanalysis (Hersbach et al., 2020), ERA5, was used as the main
126 data source in this work. The dataset is generated using 41r2 of the Integrated Forecast System (IFS) model, based

127 on a four-dimensional variational data assimilation scheme, and takes advantage of 137 vertical model levels and a
128 horizontal resolution of 0.28125° (31 km). The data provides hourly estimates of model integration. In this study,
129 hourly zonal and meridional winds (650 and 925 hPa), specific humidity (925 hPa), temperature (925 hPa), and
130 convective available potential energy (CAPE) in ERA5 during 1981–2020 were used to explore suitable large-scale
131 environments for the development of MCSs in SWA (5–9°N, 10°W–10°E). The zonal and meridional wind, ~~as well as~~
132 ~~specific humidity~~ at 925 hPa, are used to understand the penetration of monsoon flow inland. The zonal wind
133 difference between 925 hPa and 650 hPa is used as a zonal wind shear change indicator while the temperature at 925
134 hPa is used to visualize Saharan heat low (SHL) differences. Due to the main direction in which MCSs propagate
135 (east to west), enhanced easterly zonal wind shear are presented as positive anomalies as these are positively related
136 to storm development. Specific humidity (q) at 925 hPa was used to explore whether CAPE changes are controlled
137 by low-level q. We consider also the total column water vapour (TCWV) due to its ability to represent the total
138 gaseous water in the vertical column of the atmosphere which is influenced by the evolution of the humidity field.
139 TCWV represents the precipitable water the atmosphere holds better than the humidity.

140 The Meteosat Second Generation (MSG) cloud-top temperature data, which are available every 15 minutes
141 from the Eumetsat archives online (<https://navigator.eumetsat.int/product/EO:EUM:DAT:MSG:HRSEVIRI>) was
142 used in this study. Twelve years of MCS snapshots (2004–15) detected from Meteosat Second Generation 10.8 μm-
143 band brightness temperatures (Schmetz et al., 2002, EUMETSAT 2021) are used to define MCS days in this study.
144 Following (Klein et al., 2021), an MCS is defined here as a -50°C contiguous cloud area larger than 5000 km². We
145 consider the MCS images every half hour, for which they are matched up with the half-hourly Integrated Multi-
146 satellite Retrievals for Global Precipitation Measurement (IMERG; Huffman et al. 2019) dataset, using the merged
147 microwave / infra-red (“precipitationCal”) rainfall product. An “MCS day” is then defined as a day with at least one
148 hour containing 5 simultaneously existing MCSs between 16 and 1900 UTC with maximum rainfall >5mm within
149 the SWA domain. Fifteen years of MCS snapshots (2004–18) detected from Meteosat Second Generation 10.8 μm-
150 band brightness temperatures (Schmetz et al. 2002, EUMETSAT 2021) are used to define MCS days in this study.
151 Following Klein et al. (2021), an MCS is defined here as a -50°C contiguous cloud area larger than 5000 km². An
152 “MCS day” is then defined as a day with at least 5 MCSs between 16 and 1900 UTC per day that is raining >5mm
153 within the SWA domain. This can include the same MCS at several timesteps in a day. Corresponding rainfall
154 snapshots were sampled from the “high-quality precipitation” (HQ) field within the Integrated Multi-satellite
155 Retrievals for Global Precipitation Measurement (IMERG; Huffman et al. 2019) dataset. Here, only land-based
156 MCSs because MCSs over land are fundamentally more intense and deep than its counterpart over the ocean (Mohr
157 and Zipser 1996).

158

159 3 Methodology

160 3.1 Self-organising Maps (SOMs) analysis

161 The study uses the self organizing map (SOM; Kohonen 1982, 2001) from SOM-PAK-3.1 software. The
162 technique is used to identify archetype synoptic circulation patterns over the southern West Africa region by training
163 a 9-node SOM with ERA5 daily mean 925 hPa geopotential height fields to produce 9 characteristic circulation

164 patterns for the period 1981 to 2020. The geopotential height circulation pattern is used here mainly based on its
165 physically realistic output spanning a range of circulation features found in the atmosphere (Hewitson and Crane,
166 2002) and its ability to detect the West African Heat Low (WAHL) which is a key element of the West African
167 monsoon system (Lavaysse et al. 2009; Biasutti et al. 2009). The SOM is mostly the preferred choice over other
168 clustering methods such as the principal component analysis (PCA) or K-means because the data is not discretized
169 and orthogonality is not forced or does not require subjective rotations to produce interpretable patterns. The main
170 advantage of the SOM technique is its ability to deal with non-linear data (such as the continuum of atmospheric
171 conditions) and can easily be visualized and interpreted (Reusch et al. 2005; Lennard and Hegerl, 2014). The steps
172 within the technique can be broadly grouped into two stages, namely the training stage and the mapping stage.
173 Earlier studies (e.g. Hewitson and Crane 2002; Kim and Seo 2016; Lee 2017; Rousi et al. 2015; Sheridan and Lee
174 2012) have successfully used this technique in synoptic climatology to effectively preserve relationships between
175 weather states while giving outputs that are readily understood and can be easily visualized as an array of classified
176 patterns. These classified patterns help in interpreting relationships between large-scale regional circulation patterns
177 and local weather expressions and rainfall extremes (Hewitson and Crane 1996; Cassano et al. 2015; Wolski et al.
178 2018). In this study, the SOM is randomly initialized allowing for hidden patterns and structure in the geopotential
179 height at 925 hPa to be discovered while the algorithm iteratively updates the weights of the nodes to better
180 represent the data. The strength of initializing the SOM this way lies also on its robustness to noise and outliers as a
181 result of the algorithm applying a competitive learning structure to the data which then allows for the formation of
182 distinct clusters. The SOM_PAK algorithm allows the SOM process to minimize quantization and topological errors
183 at the mapping stage when choosing the best SOM as outlined in Lennard and Hegerl (2014). However, there is a
184 trade-off when choosing the size of the SOM, as this is dependent on the need to generalize circulation states for
185 analyses or the need to capture predominant spatial characteristics that affect the local climate. Thus, in this study,
186 we have tested several sizes of the SOM and have arrived at using a 9-node SOM. As depicted in Fig. S1 for a 9-
187 node SOM, it is evident that some nodes are still redundant, and this is a compromise on states not being overly
188 generalized while capturing the dominant spatial characteristics over the region. Here, we agree on six nodes, which
189 allow distinct synoptic states to be reproduced while grouping nodes that are similar. This grouping was done based
190 on similarities in atmospheric patterns and seasonal frequency from the 9-node case. The choice of how many SOM
191 nodes to choose is a trade-off between distinctiveness and robustness. Based on SOM_PAK, we tested node sizes
192 2x3, 3x3, and 3x4, using the quantization error (QE) as an indicator of the quality and robustness of the respective
193 node size. We find a minimized QE for 3x3 (c.f. Supplementary Figure S1), which, from visual inspection, also
194 shows a larger number of distinct circulation features than 2x3 while producing fewer redundancies than 3x4. Thus,
195 all the following analyses are based on the 3x3 node matrix.

196

197 3.2 Large-scale WAM patterns on southern West Africa MCS days

198 Based on the 6 different large-scale node patterns, we explore within-node large-scale conditions that
199 characterize MCS days in SWA. For examination of environmental conditions suitable for SWA MCS activity,
200 large-scale conditions were taken from hourly ERA5 reanalysis data sampled at 1200 UTC when the daily

201 convective activity is more representative of pre-convective atmospheric conditions (Klein et al. 2021). Pre-
202 convective conditions are considered in the study to reduce the effects of feedback from the MCSs on environmental
203 conditions (Song et al. 2019). Composites of ERA5 large-scale environmental variables (temperature, wind, specific
204 humidity, and CAPE) are created for all node days, and for MCS days within each SOM node. Finally, the anomaly
205 in large-scale patterns between MCS days and node mean conditions are computed to determine MCS-favourable
206 adjustments in large-scale patterns within each node. A two-sided Student's t-test is used to determine significant
207 differences between node climatologies and MCS-day sub-samples.

208 In addition to large-scale condition composites, we also sample pre-convective (1200 UTC) local
209 atmospheric conditions (ERA5), for each 1800 UTC MCS at the location of minimum cloud top temperature. We
210 only consider 1800 UTC MCSs for local condition sampling to avoid oversampling similar atmospheric states from
211 several MCS time steps. These conditions are compared to the node climatology conditions at the same locations,
212 allowing us to explore the difference in node climatology versus MCS day conditions at the specific locations where
213 MCSs occurred on respective days. Here we only focus on the afternoon peak of convection when it is triggered and
214 is in early stages of organization. It should be noted that driver importance may shift for nocturnal MCSs in later
215 hours, when CAPE is reduced over night and shear may increase further in importance for MCS maintenance (Vizy
216 et al, 2018)

217

218

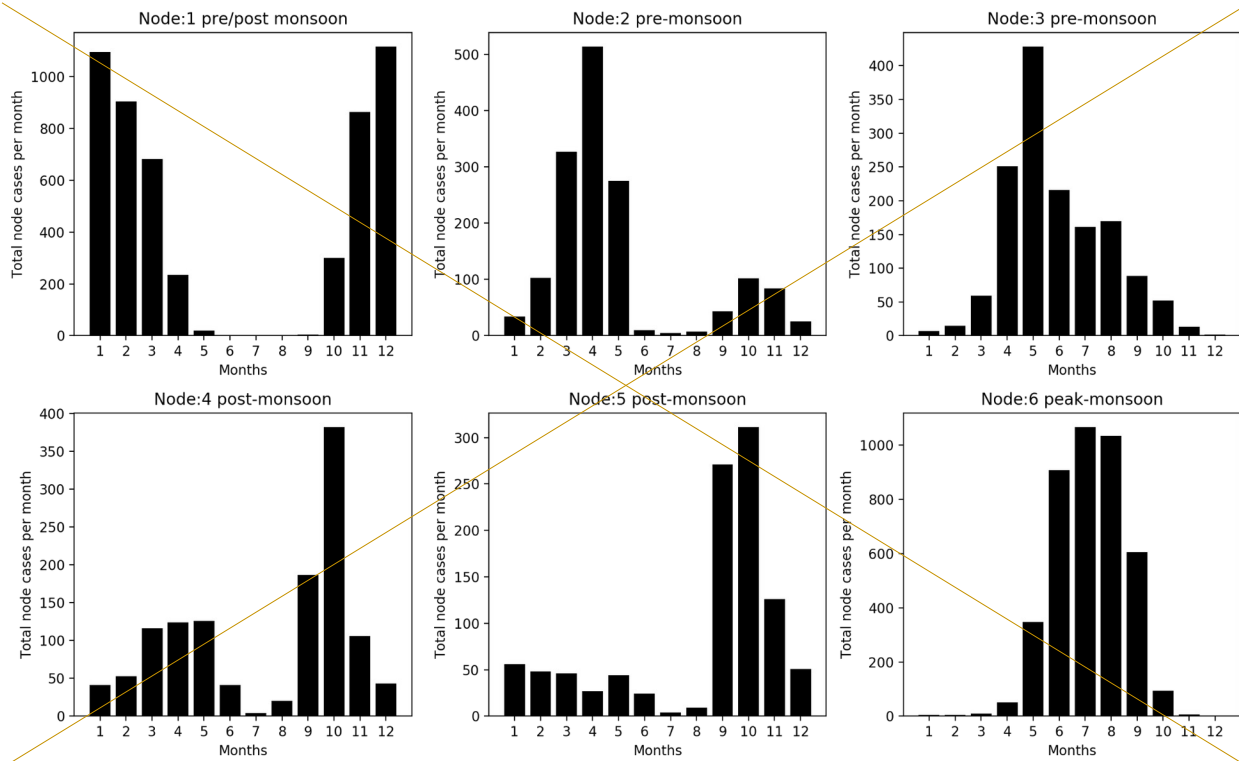
219 4 Results

220 4.1 Node seasonality and mean conditions

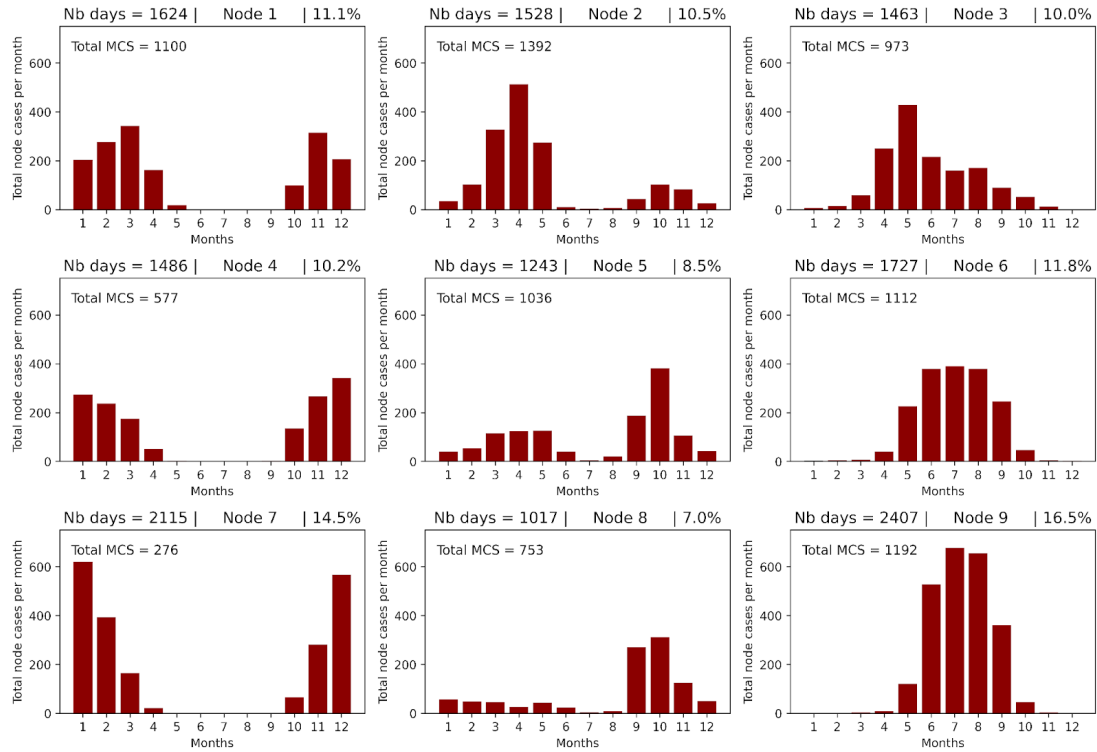
221 A 9-node SOM (Fig. 1) with distinct synoptic states was identified, where the nodes are hereafter referred
222 to as nodes one (1) to nine (9). Considering the SOM node frequency distributions in Fig. 1, it is noticeable that the
223 nodes separate different stages of the monsoon circulation seasonality, although certain nodes evidently cover a
224 wider range of months that cannot be represented by the typical monthly grouping of the seasonal cycle (e.g.
225 2,3,5,8). In analyzing the 9-node SOM (Fig. S1), six SOM nodes (Fig. 1) with distinct synoptic states were
226 identified and were further associated with being either a pre-, post-, or peak-monsoon synoptic circulation type as a
227 result of which months in the year they dominantly occur. This was done based on similarities in atmospheric
228 patterns and seasonal frequency from the 3 X 3 node SOM. These nodes are hereafter referred to as nodes one (1) to
229 six (6). The SOM nodes are noted to generally represent patterns of the seasonal cycle of monthly rainfall amounts.
230 Circulation patterns in nodes 1, 4, and 7 can be attributed to cases primarily observed in the first three months
231 (January, February, and March) and the last two months (November, and December), hence a pattern most
232 representative of the dry season months. It is noted that On the other hand, nodes 2, 5, and 8 depict an environment
233 that is prominent during the pre-monsoon and the post-monsoon seasons, with node 2 presenting a clearer seasonal
234 exclusivity during pre-monsoon while nodes 5 and 8 shows frequent occurrences throughout during the post-
235 monsoon season. Patterns of node cases significant in the post-monsoon season are observed in nodes 4 and 5.
236 However, node 4 evidently shows transition patterns that have frequent occurrences in both pre and post-monsoon
237 seasons although most prominent in the post-monsoon season. These nodes (nodes 2, 5, and 8) are hence in the

238 following referred to as transition season nodes, a period that connects the dry and monsoon season. The right-hand
 239 side of the SOM nodes 3, 6, and 9 represent patterns that cover monsoon season months, but can similarly feature
 240 high frequencies outside of the monsoon season (e.g. node 3 with the highest frequency in May). Patterns in node 6
 241 are more strongly related to peak monsoon conditions:

242
 243



244



245

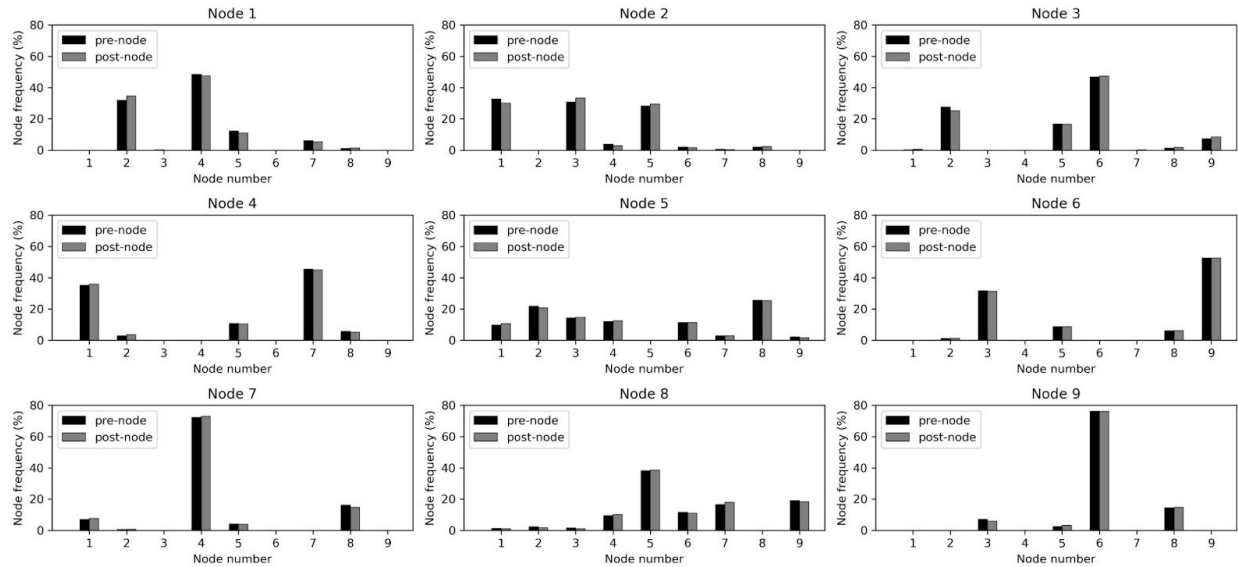
246

247

248 **Figure 1.** Monthly distribution of node cases based on SOM analysis. Bar values indicate the total number of MCSs
 249 per month from 2004 to 2015. The total number of MCS per node from 2004 to 2015 is displayed in node panels.
 250 The title shows the total number of days in each node (left) and the contribution of each node to the total node days
 251 (right).

252

253



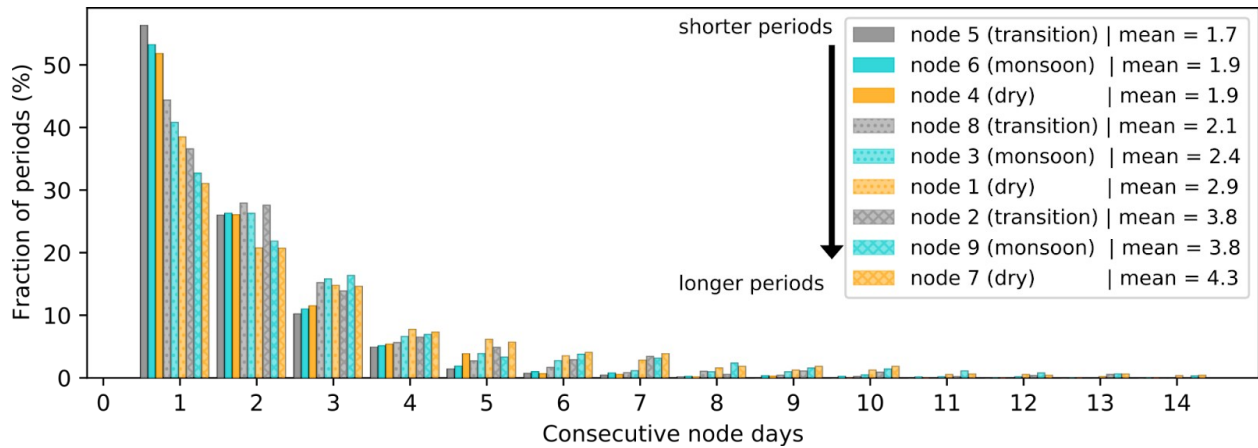
254

255 Figure 2: Frequency of nodes (%) preceding (pre-node) or following (post-node) each of the nine nodes.

256

257 To investigate the relationship between nodes across our 3x3 SOM matrix, we now consider the
 258 frequencies at which node states are preceded or followed by other nodes in Fig. 2. The resulting frequency
 259 distributions reinforce a classification of the matrix columns into dry (1,4,7), transition (2,5,8) and monsoon (3,6,9)
 260 season nodes, with the top row (1,2,3) representing nodes that are preceded or followed by nodes of a different
 261 season (column) 20-30% of the time. The bottom row nodes (7,8,9) on the other hand are distinct within-season
 262 states that are almost never connected to first row nodes (1,2,3) but are reached via intermediate middle row nodes
 263 4,5,6. The node matrix separates different season states along rows, while columns seem to represent within-season
 264 states where upper and lower rows are separate states, temporally connected by conditions captured by middle-row
 265 nodes. Finally, the persistence of nodes presented in Fig. 3 reflects the discussed matrix structure, with connecting
 266 middle-row nodes 4,5,6 featuring shortest periods with on average 1.7-1.9 days, suggesting more transient states.
 267 Nodes 2,9,7 on the other hand show the smallest number of single day occurrences (consecutive node days = 1),
 268 pointing towards more stable, persistent conditions with an average period length of 3.8-4.3 days. Regarding node
 269 characteristics, it is striking that each seasonal node group features nodes of differing persistence (c.f. node season
 270 order for consecutive node days = 1), rendering node persistence a key difference between same-season nodes in the
 271 SOM matrix columns.

272



273

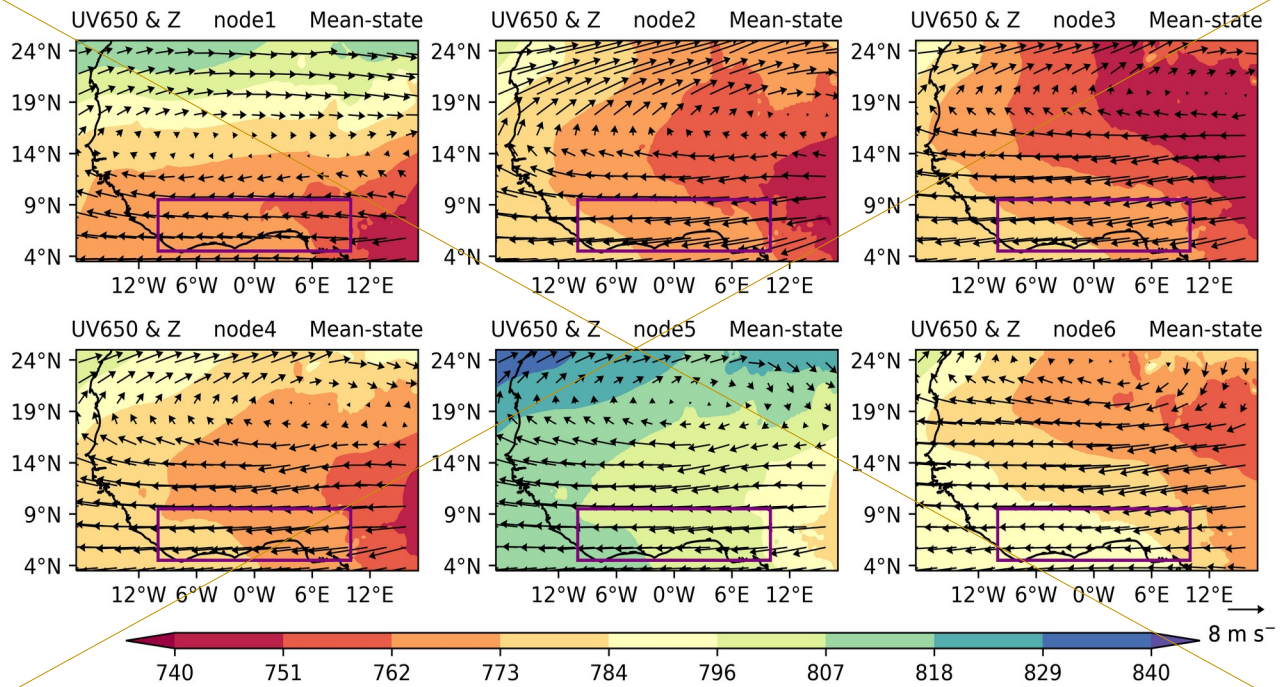
274 Figure 3: Fraction of periods covering consecutive days of different lengths per node, with the total percentage for 1-
 275 14 consecutive node days adding up to 100% per node. The node bars are ordered according to the period fraction
 276 for "consecutive node days = 1", revealing the node order going from shorter to longer temporal node persistence, as
 277 shown in the legend.

278

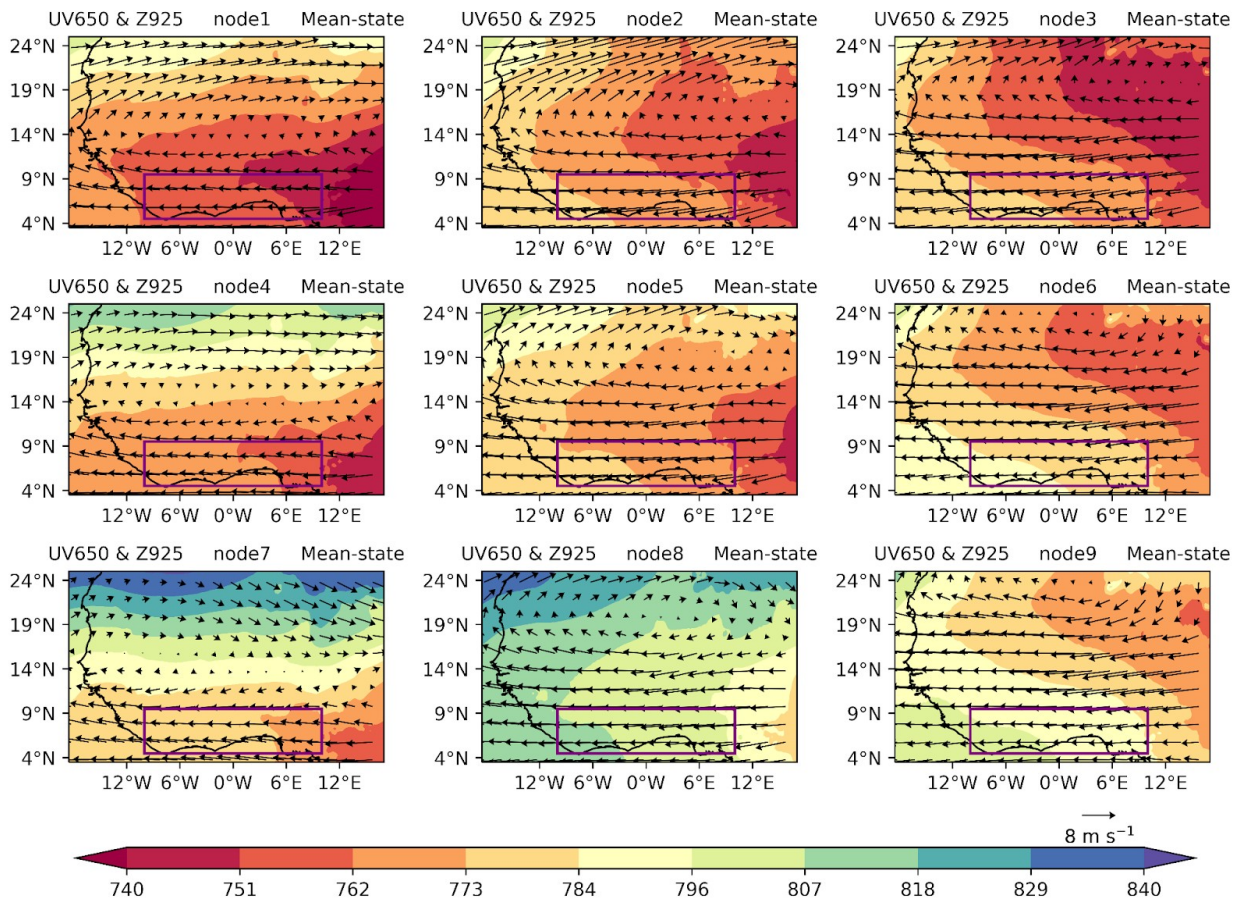
279 In the following, we inspect the average atmospheric conditions associated with the identified nodes. The
 280 SOM classification of different synoptic states was based on 925 hPa geopotential heights, with resulting patterns
 281 shown in Fig. 24. The patterns clearly show the signature of the well-known West African Heat Low (e.g. Lavaysse
 282 et al. 2009) moving northwards, strengthening over the course of the annual WAM cycle (from nodes 1, 2, and 3)
 283 and peaking in August, evident as an area of highlow pressure over the Sahara in nodes 3, 6, and 9. Nodes 4, 7, and
 284 8 show stages of the weakening of the heat low post-monsoon, coinciding with a southward movement of the 925
 285 hPa highlow pressure area and linked southward retreat of mid-level easterly winds compared to node 6. The
 286 overlaid 650 hPa wind field reveals mean easterly wind conditions at MCS steering levels across all nodes,
 287 suggesting that the dominant propagation direction for MCSs remains east to west for all identified synoptic states.

288

289



290
291

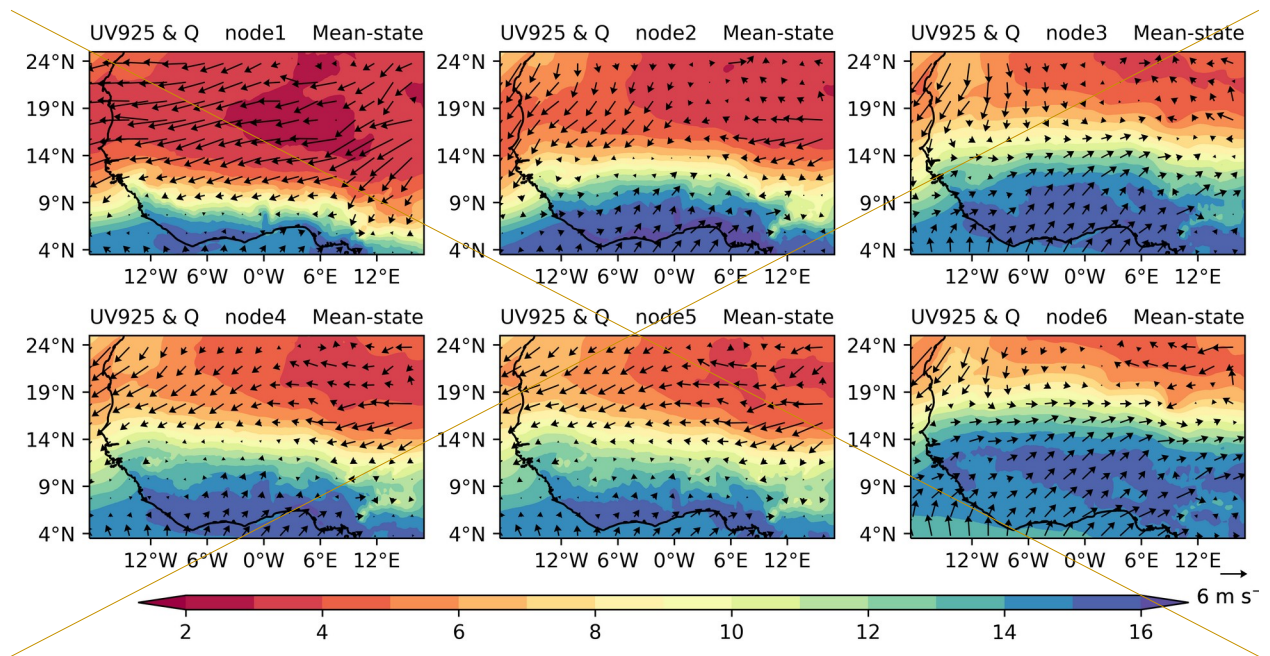


292

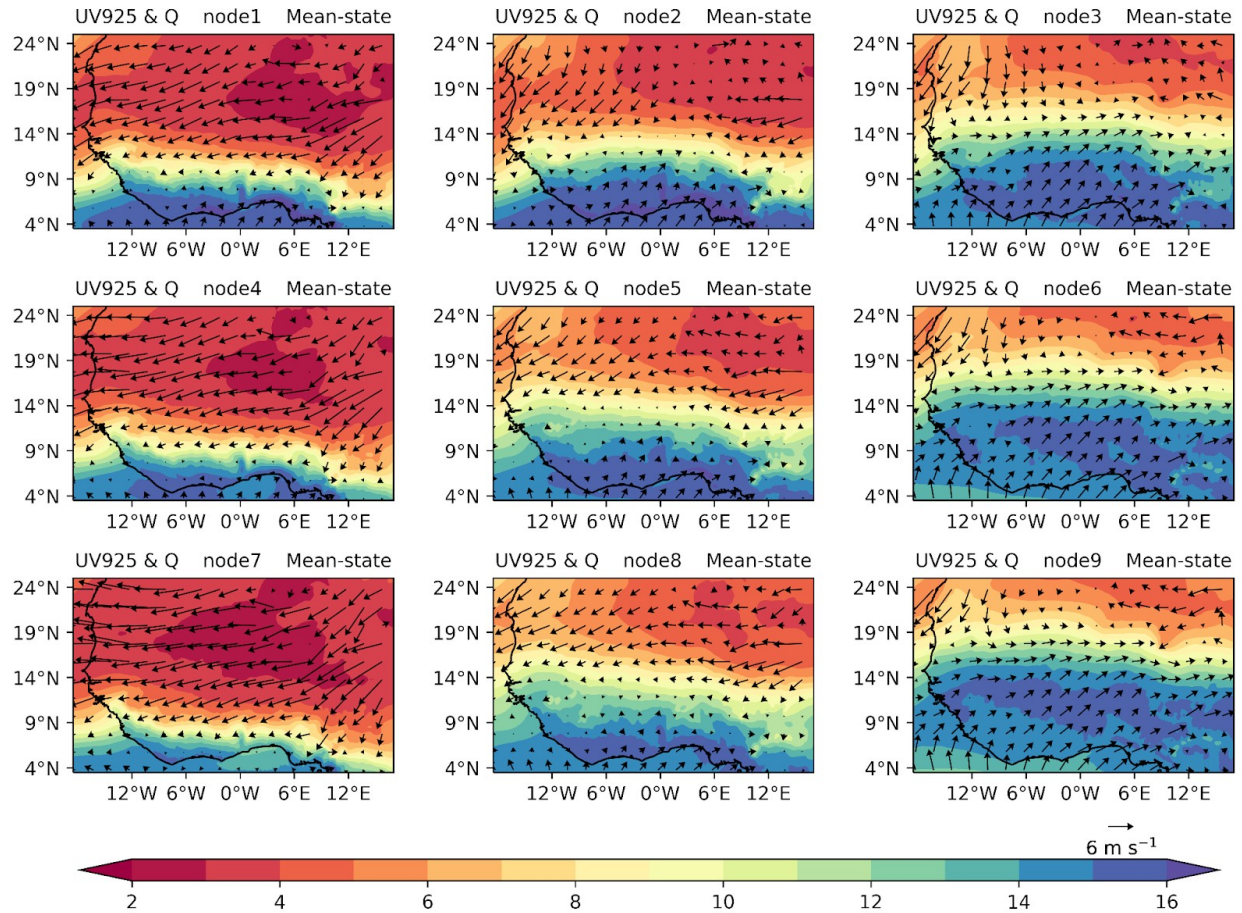
293
294
295
296
297
298
299
300
301
302
303
304
305
306
307
308
309

Figure 24. 12 UTC composites of 925-hPa geopotential height (shading; gpm) and 650-hPa winds (vectors; m s^{-1}) in six nodes based on SOM analysis. The purple box depicts the SWA region (5° – 9° N, 10° W– 10° E)

We now examine **surface** winds and moisture flows **at 925 hPa** to explore their behaviour under the **six** distinct circulation types identified (Fig. 35). In **the first nodes 1, 4, and 7**, the north-easterly winds dominate most of West Africa, with weak southerlies over SWA. This pattern in moisture distribution is evident in the dry season over West Africa, signaling a low moisture presence. The enhanced moisture observed in coastal areas of SWA can be attributed to the penetration of southerly winds. In **pre-monsoon the transition** node 2, the southerly winds strengthen and move inland, causing the north-easterly winds to retreat. A similar effect is observed in nodes **3, 4, 5** and **8** where the north-easterlies become weaker. In nodes **3, 6, and 9**, the south-westerlies are intensified and move inland, further enhancing moisture flow from the South Atlantic towards the land, representative of **peak** monsoon flow. Wind patterns for **low** mid- and **mid** low-levels (Figs. 24 and 35) illustrate vertically-sheared conditions coinciding with regions of high low-level specific humidity in all nodes (purple in Fig. 35), thus marking regions where atmospheric conditions may allow MCS development.



310



311

312

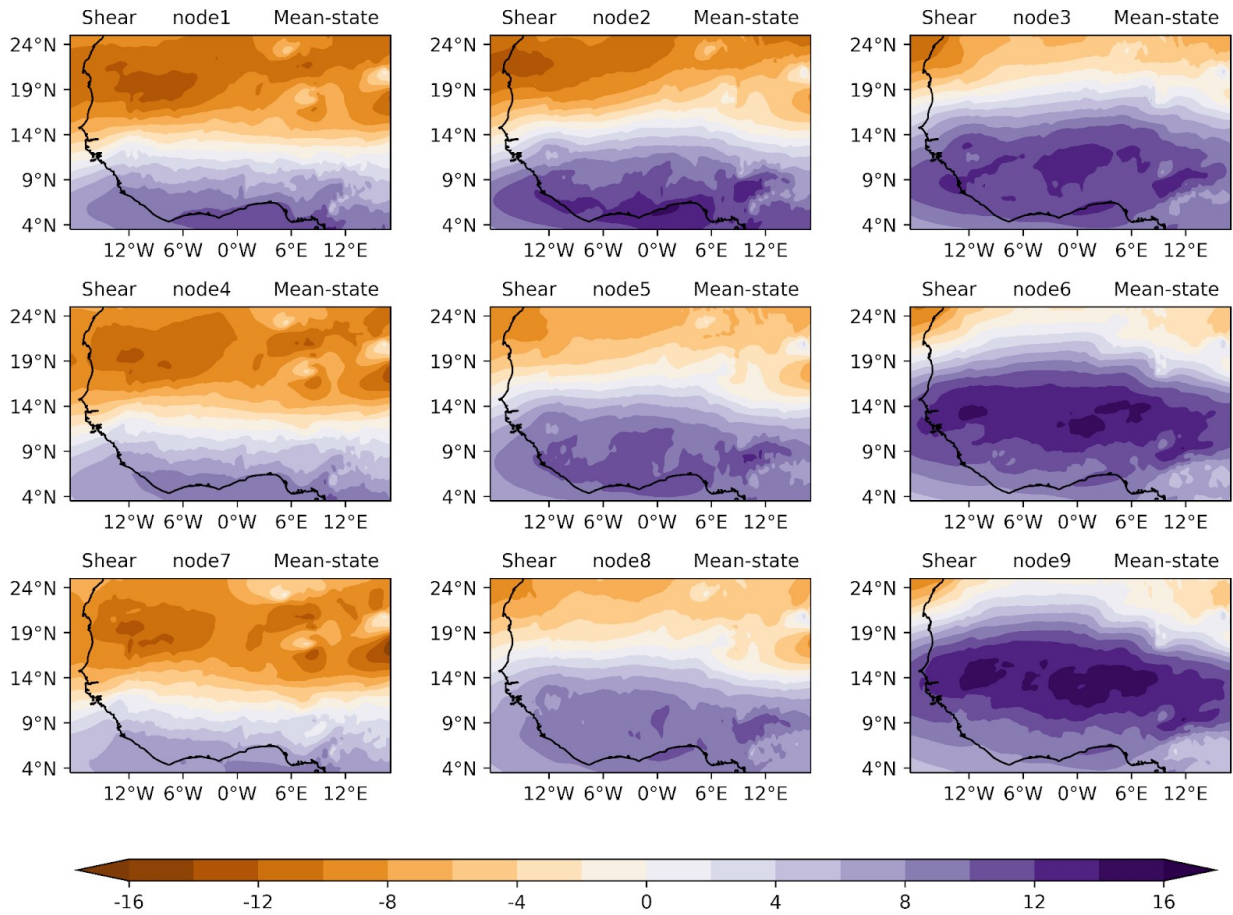
313 **Figure 35.** 12 UTC composites of specific humidity (shading; g kg^{-1}) and 925-hPa winds (vectors; m s^{-1}) in six
 314 nodes based on SOM analysis.

315

316 A further investigation was conducted to ascertain the spatial distribution of mean zonal wind shear over SWA (Fig.
 317 46), where easterly shear is represented with a positive sign in this study as it is easterly shear that contributes to
 318 MCS development in this region.- The patterns in zonal wind shear demonstrate northward transport during the
 319 propagation of the WAM cycle and a wider spread of zonal wind shear as it moves further inland (nodes 1, 2, and
 320 3). These patterns closely follow the southern boundary of weaker geopotential heights representative of high-
 321 pressure areas (Fig. 2). During from first to third column nodes illustrate a strong link of high-shear areas to the
 322 propagation of the WAM cycle, and these areas widen as the zonal shear band moves further inland. High-shear
 323 areas also closely follow the northern boundary of increased low-level humidity, marking the areas where humidity
 324 and shear conditions may allow MCS development. For nodes with high frequency in the monsoon season (nodes 6
 325 and 9-6), zonal wind shear peaks lies clearly to the north of the SWA domain. A southward retreat of zonal wind
 326 shear is observed during the post-monsoon season (nodes 4 and 5, 5, and 8). Generally, the presence of zonal wind
 327 shear can be seen as a necessary condition in the WAM system.

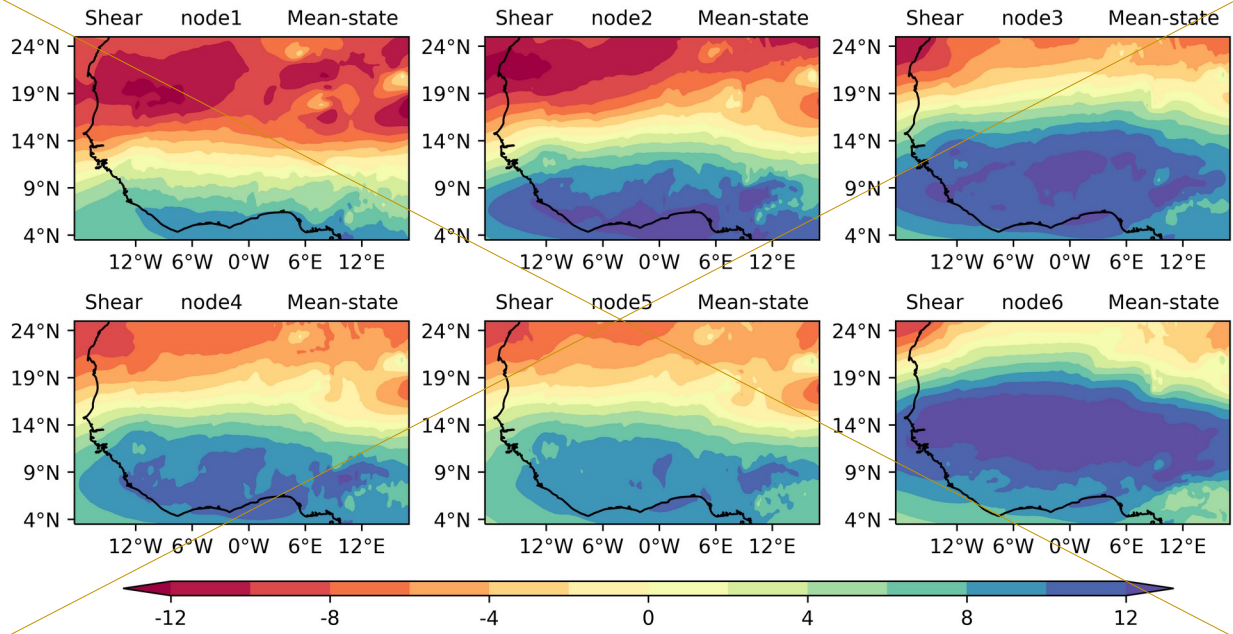
328

329



330

331



332

333

334 **Figure 46.** 12 UTC composites of zonal wind shear in six nodes based on SOM analysis.

335

336 4.2 Large-scale conditions favouring MCS days

337 The environmental conditions that are associated with favouring MCS occurrence are described in this section.

338 Firstly, the monthly climatology of MCS frequency as captured by our MCS snapshots (average number of MCSs at

339 1800 UTC across SWA domain) is considered with a focus on rainfall months in Fig. 7, which shows a

340 pronounced annual cycle of MCS numbers with frequency peaks in JuneApril and SeptemberOctober is observed

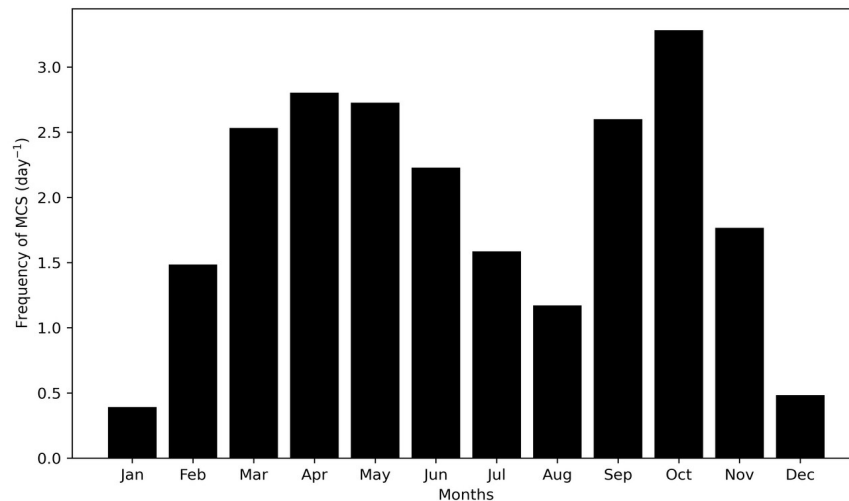
341 (Fig-5). These peak months are associated with maximumthe start of rainfall during the major rainy season and the

342 maximum rainfall for the minor rainy seasons across SWA respectively. The monthly climatology of MCS

343 frequency decreases from JuneApril to August, with August being the local minimum. This local minimum

344 corresponds to the so-called “little dry season” (Le Barbé et al., 2002; Vollmert et al., 2003) that exists before the

345 southward retreat of the rainbelt.



346 **Figure 57.** Average annual cycle of MCSs at 1800 UTC within the SWA box showing the monthly average of MCS
347 number per day.

348

349 The spatial distribution of MCS frequencies during node days is depicted in Fig. 8. Comparing daily MCS

350 frequencies, we find that MCSs are most likely to develop under transition node (2,5,8) conditions (2.8 MCSs per

351 day) featuring a northward-displaced moisture anomaly (Fig. 9). Given the transition nodes occur predominantly

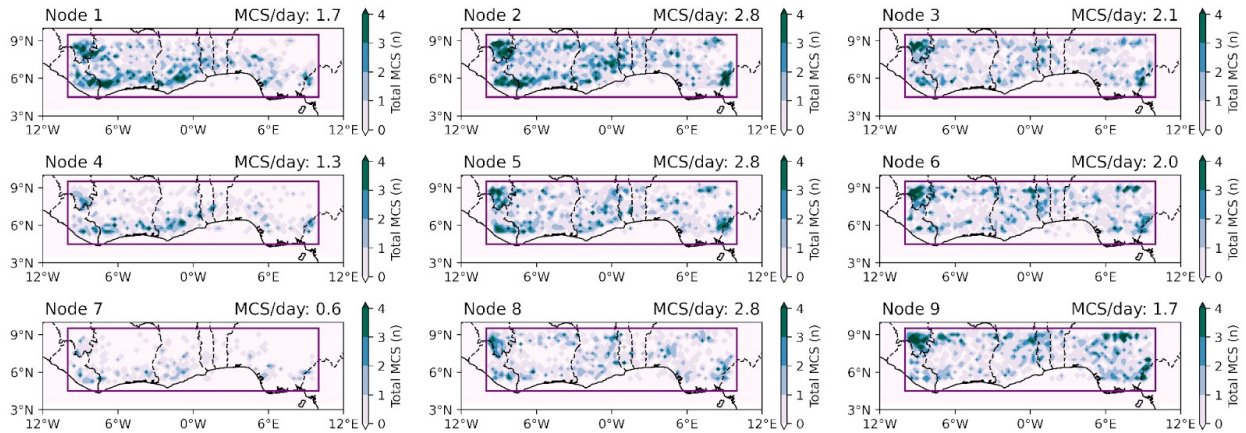
352 during pre-monsoon (late March to June) and post-monsoon (from September to November) - the major and the

353 minor rainy season respectively in SWA (cf. Fig.~1), these patterns may in some cases be representative of early

354 monsoon onset and a delayed monsoon retreat respectively. MCSs more rarely develop under dry node (1,4,7)

355 conditions, with frequencies as low as 0.6 MCSs per day.

356



357

358

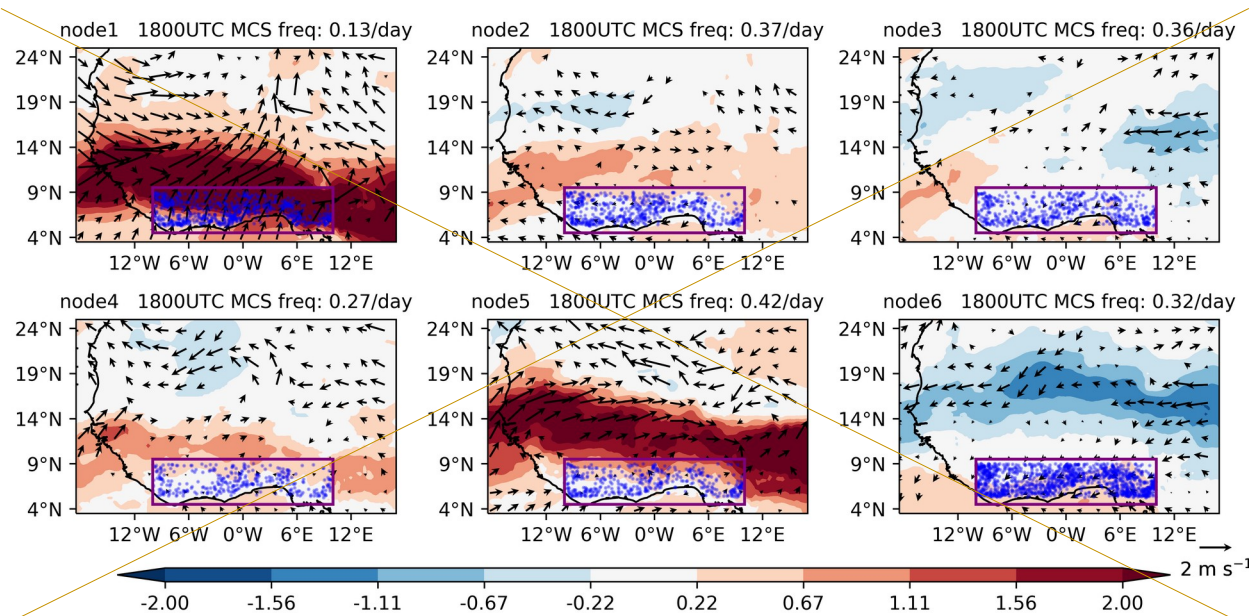
359

360

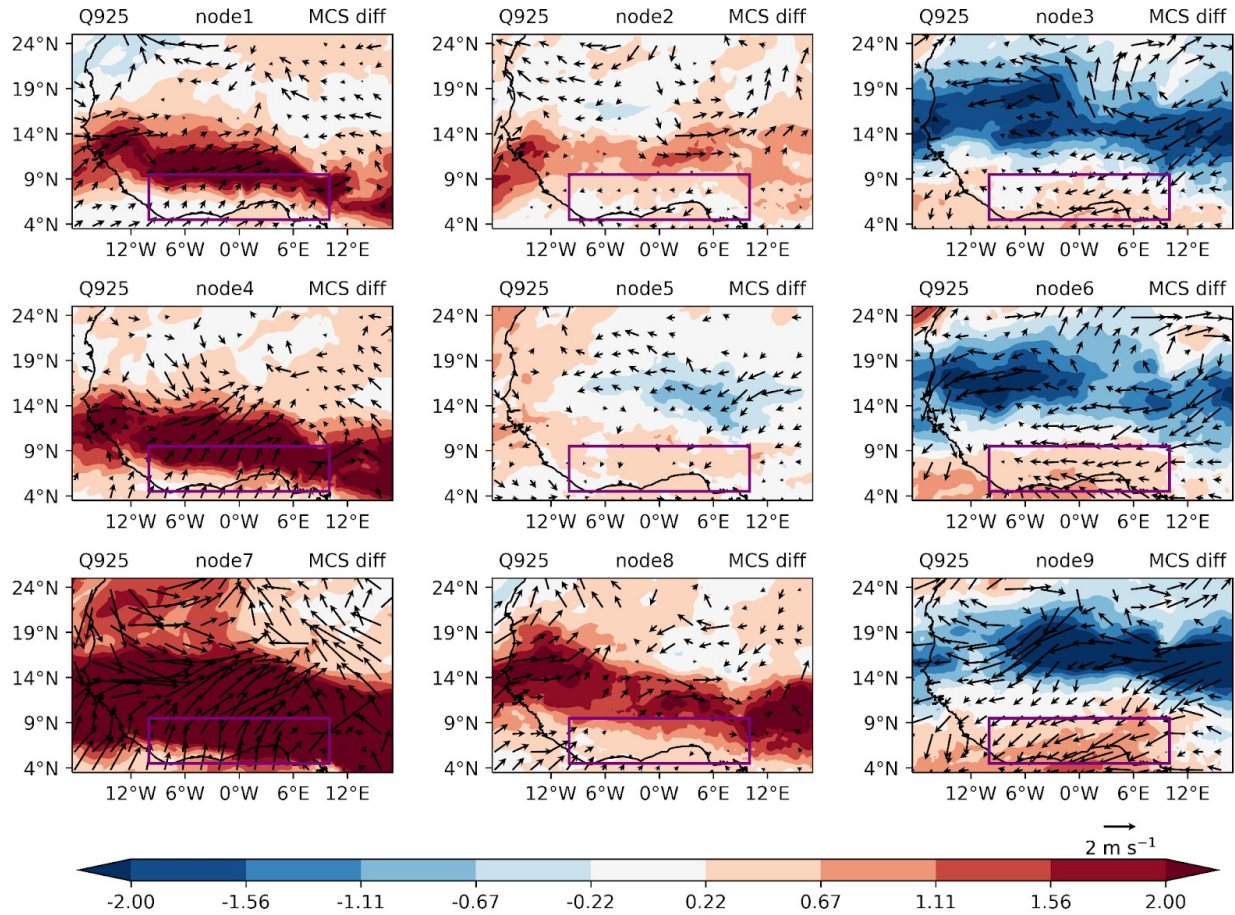
361

362

Figure 8. The SWA region indicating the spatial distribution of MCSs during node days. The purple box depicts the main study region of southern West Africa (SWA, 10°W - 10°E, 5-9°N) and titles show the frequency of MCS per day per node within the SWA box.



363



364

365

366 **Figure 69.** 12 UTC MCS-day composite anomalies of specific humidity (shading; g kg^{-1}) and 925-hPa winds
 367 (vectors; m s^{-1}) in six nodes based on SOM analysis. The purple box depicts the SWA region ($5^{\circ}\text{--}9^{\circ}\text{N}$, $10^{\circ}\text{W--}10^{\circ}\text{E}$)
 368 and the blue dots indicate the location of MCSs during node days. Specific humidity anomalies are shown when they
 369 are significant at the 5% level; wind vectors are shown when either the zonal or meridional wind anomalies are
 370 significant at the 5% level.

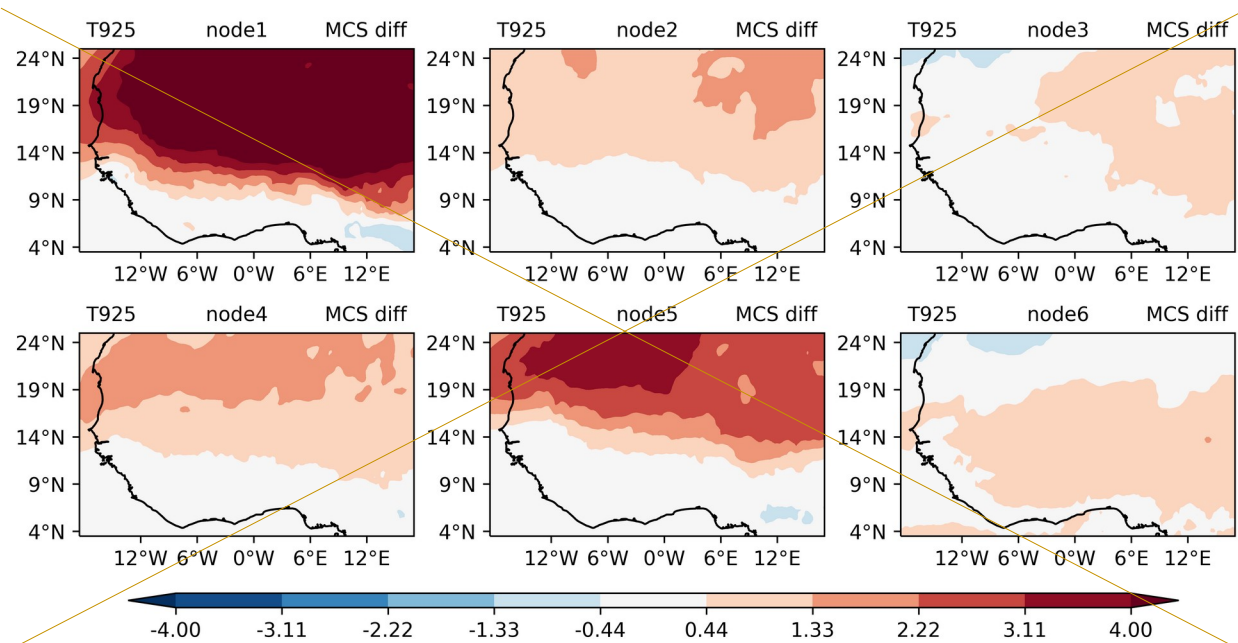
371

372 During the dry season nodes 1, 4, and 7, a positive widespread moisture anomaly is
 373 observed with anomalous south-westerly winds over SWA (Fig. 69). This depicts a substantial enhancement in the
 374 low-level moisture transport during a result of the few days of with convective activities during the dry season. In
 375 the transition nodes 2, 3, 4, and 5 (2, 5, 8), low-level moisture anomalies during convective activity days show weak
 376 and mostly insignificant behaviour along the SWA coast based on the two-sided Student's t-test. In node 5, a
 377 positive moisture anomaly is located over the northern part of SWA. During monsoon nodes (3, 6, 9), a notable
 378 region of anomalous low-level easterly winds and also the seemingly partly northerlies from the Mediterranean
 379 region coincides with negative moisture anomalies is observed over the Sahel, indicating a weakening of the south-
 380 westerly monsoon winds and of the low-level westerly jet, which reduces moisture transport towards the Sahel.
 381 Strong easterly winds during MCS days reduce the moisture over the Sahel but introduce more moisture over the

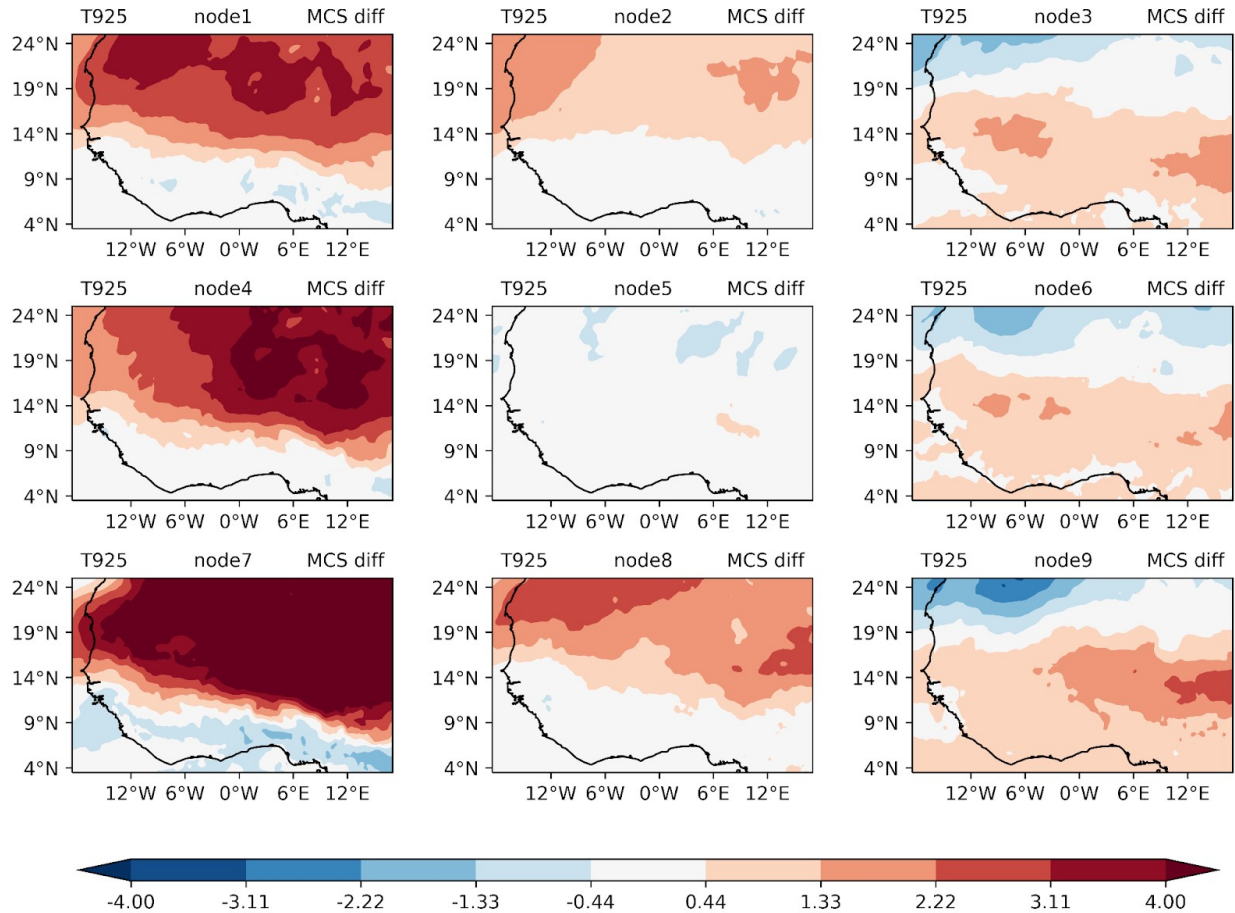
382 coast. Comparing daily MCS frequencies, we find that MCSs are most likely to develop under node 5 conditions
 383 featuring a northward-displaced moisture anomaly (0.42 MCSs per day), linked to strengthened low-level westerlies.
 384 Given this node occurs predominantly from September and into November – the minor rainy season in SWA (cf.
 385 Fig. 1), these patterns may in some cases be representative of a delayed monsoon retreat. This is evident in the
 386 negative moisture anomalies over the Sahel and the increase in moisture over the coastal regions during MCS days,
 387 which can result in less convective activities over the Sahel region and more convective activities over coastal areas.

388 We now consider low-level temperature anomalies to detect potential changes in temperature gradients and
 389 SHL strength on MCS days. Figure 710 shows a widespread increase in temperature north of SWA during days with
 390 active convection in the dry (1,4,7) and transition (2,8) nodes, which may explain strengthened south-westerly wind
 391 anomalies in some of these nodes (c.f. Fig. 9) 1, 2, 4, and 5. The SWA region itself in the dry and transition nodes,
 392 on the other hand, reveals a negative and/or insignificant change in temperature during MCS days when compared
 393 with the mean climatology. Indeed, for nodes 1 and 5 this coincides with low-level westerly wind south of 15N (cf.
 394 Fig. 6). In monsoon nodes 3, 6, and 9, temperatures are enhanced in most parts of West Africa including SWA
 395 during days with active convection.

396
 397



398



399

400

401 **Figure 710.** 12 UTC composite anomalies of 925hPa temperatures (°C) in ~~six~~9 nodes based on SOM analysis.

402 Temperature anomalies are shown when they are significant at the 5% level.

403

404

405 Figure 811 shows the spatial distribution of zonal wind shear anomaly between days with convective MCSs

406 over SWA and the climatological zonal wind shear mean for the 69 different nodes across West Africa. Generally,

407 all dry and transition nodes except node 65, reveal a widespread increase in zonal wind shear anomaly over West

408 Africa with the dry nodes 1 and 5 depicting stronger events. Zonal wind shear anomalies tends to be stronger during

409 the dry and early part of the major rainy season (node 1) with theirits peak partly over SWA, but resides to the north

410 of SWA during the minor rainy transition seasons (nodes 42 and 58); in line with previously identified zonal wind

410 shear seasonality for the region (Klein et al. 2021). The positive shear anomaly patterns align with patterns of

411 strengthened temperature gradients for respective dry and transition season nodes (c.f. Fig. 10): only node 5 shows

412 no large-scale temperature anomalies and consequently patchy changes in shear, while strongest shear increases

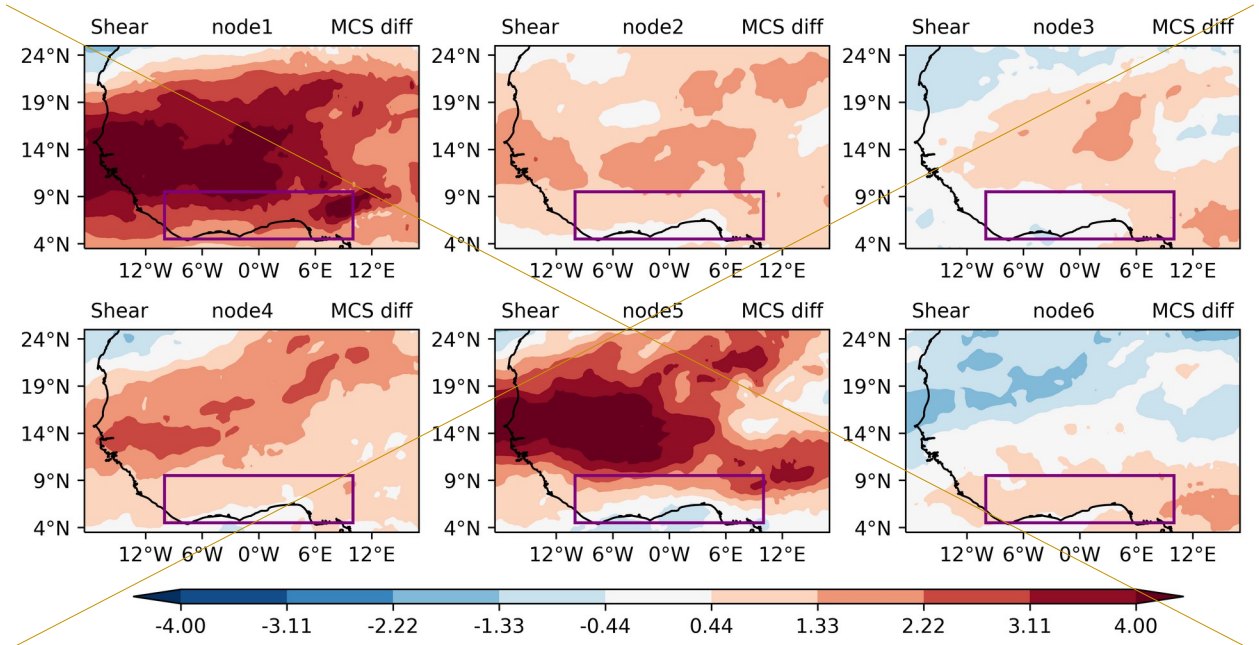
413 occur for node 7 alongside the highest temperature gradient increase. Nodes 42 and 58 (post-monsoon) however still

414 experience an appreciably significant increase in zonal wind shear over SWA for MCS days during the minor

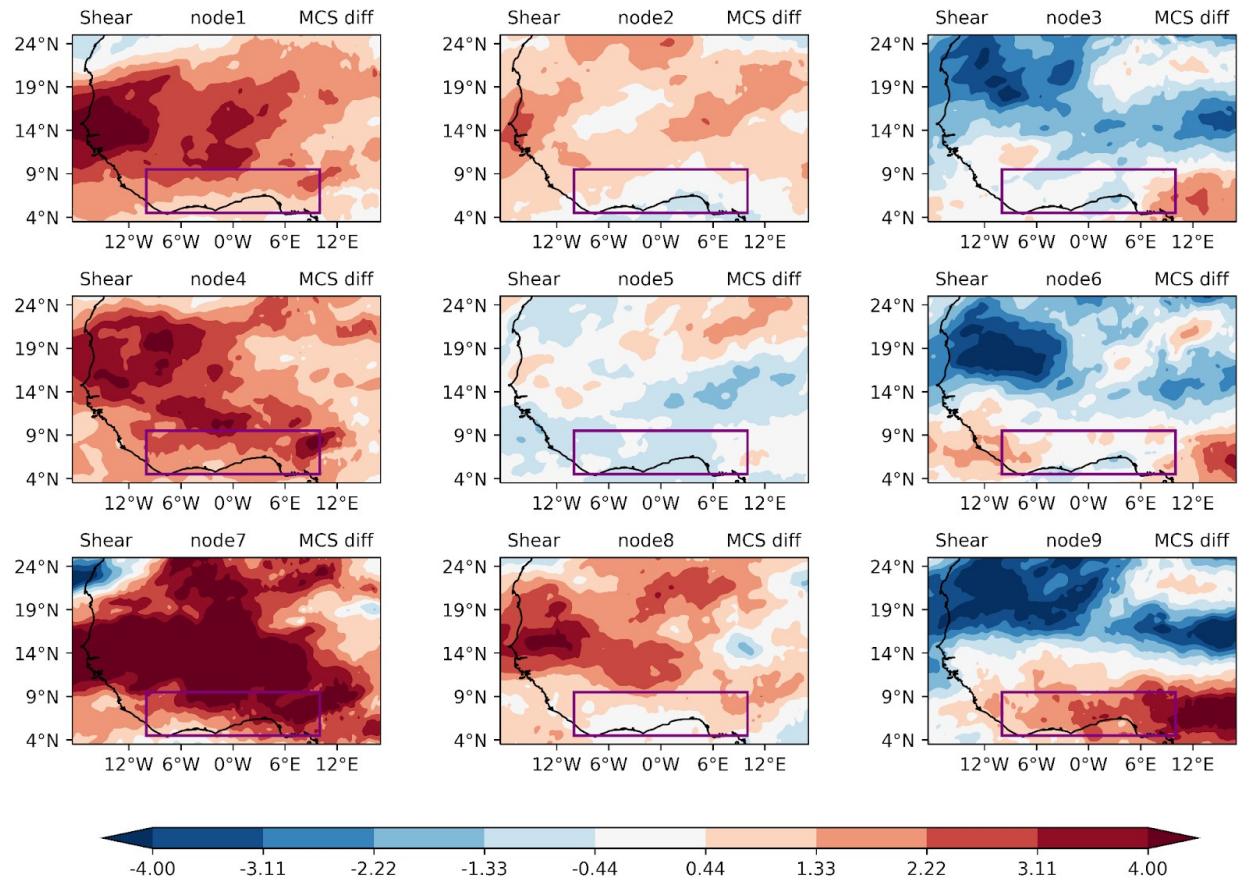
415 rainy transition seasons. Node 6The monsoon nodes (3,6,9), on the other hand, exhibits a significant increase in zonal

416 wind shear mainly confined to the south with a pronounced signal in node 9SWA associated with a peak in eastern-

417 Sahel warming (Fig. 10). In line with the expected zonal wind shear response to an increased large-scale meridional
 418 temperature gradient, we thus find the strongest zonal wind shear anomalies for nodes with strongest positive low-
 419 level temperature anomalies to the north of SWA (nodes 1, 54,7; followed by nodes 2, 48), highlighting that a warmer
 420 Sahel can promote MCS-favourable shear conditions in SWA, particularly in the pre- and post-monsoon seasons.
 421
 422



423
 424



425

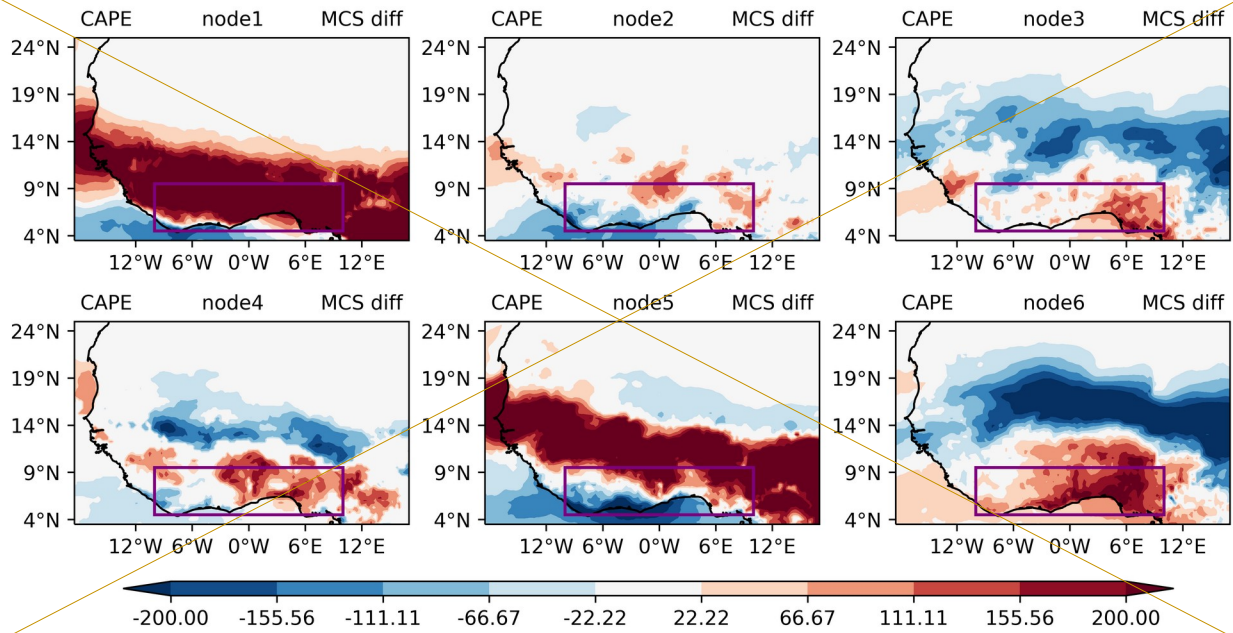
426 **Figure 811.** 12 UTC composite anomalies of zonal wind shear (m s^{-1}) in ~~six~~9 nodes based on SOM analysis. zonal
 427 wind shear anomalies are shown when they are significant at the 5% level.

428

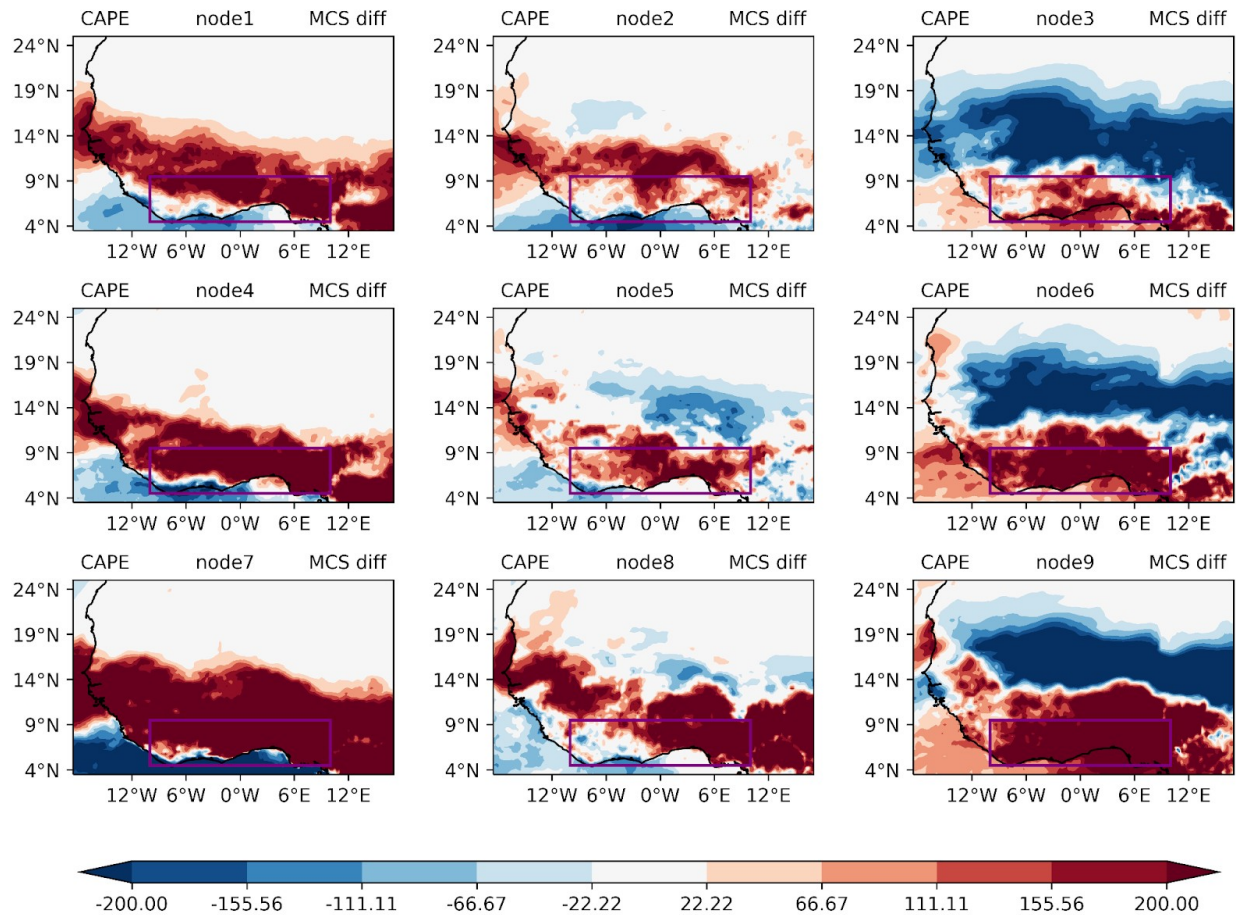
429 Investigating the first-order condition for convection development, we also evaluate CAPE for a parcel at
 430 925 hPa to ascertain the level of increased MCS-day instability in various nodes over SWA (Fig. 912). A large strip
 431 of higher CAPE values extending over the entire region of SWA and the southern Sahel from 5°N–15°N is observed
 432 (~~node 1~~dry and transition nodes). This large strip of higher CAPE is situated ~~further north~~mainly in central and east
 433 of SWA ~~for node 5~~, while part of the western coast tends to depict patterns of lower CAPE values, suggesting
 434 increased MCS likelihood only for ~~the central and~~ eastern parts of the domain. ~~During monsoon nodes~~, node 3
 435 shows a swath of high CAPE values in particular to the ~~east coast~~ and in some instances extends to the ~~central~~entire
 436 SWA (node 46) and ~~south-western parts~~north of SWA (node 69). ~~For nodes 3-6~~, ~~h~~Higher CAPE conditions over
 437 SWA are to differing degrees significantly associated with decreased CAPE in the Sahelian region, creating a dipole
 438 pattern that can occur during ~~pre-, peak- and post-monsoon~~transition and monsoon periods according to node
 439 frequencies (cf. Fig 1). Overall, all nodes show positive CAPE ~~and negative convective inhibition~~ (c.f.
 440 ~~Supplementary Fig. S5~~) anomalies for MCS_days in parts of SWA, creating an environment sufficiently unstable to
 441 support the development of convection. ~~It can be said that regions over SWA that exhibit a higher CAPE on MCS~~
 442 ~~days also depict stronger zonal wind shear~~ (Fig. 8). Indeed, it has previously been shown that colder, more intense
 443 MCSs predominantly occur under conditions with high CAPE and high zonal wind shear anomalies (Klein et al,

444 2021), which we show is consistent across all classified large-scale patterns. The close alignment with regions of
445 increased low-level humidity (Fig. 9) suggests increased low-level moisture advection as the main driver for these
446 instability changes.

447
448
449



450



451

452 **Figure 912.** 12 UTC composite anomalies of CAPE (J kg^{-1}) for MCSs occurring in each type of large-scale
 453 environment determined by the SOM analysis over SWA. CAPE anomalies are shown when they are significant at
 454 the 5% level.

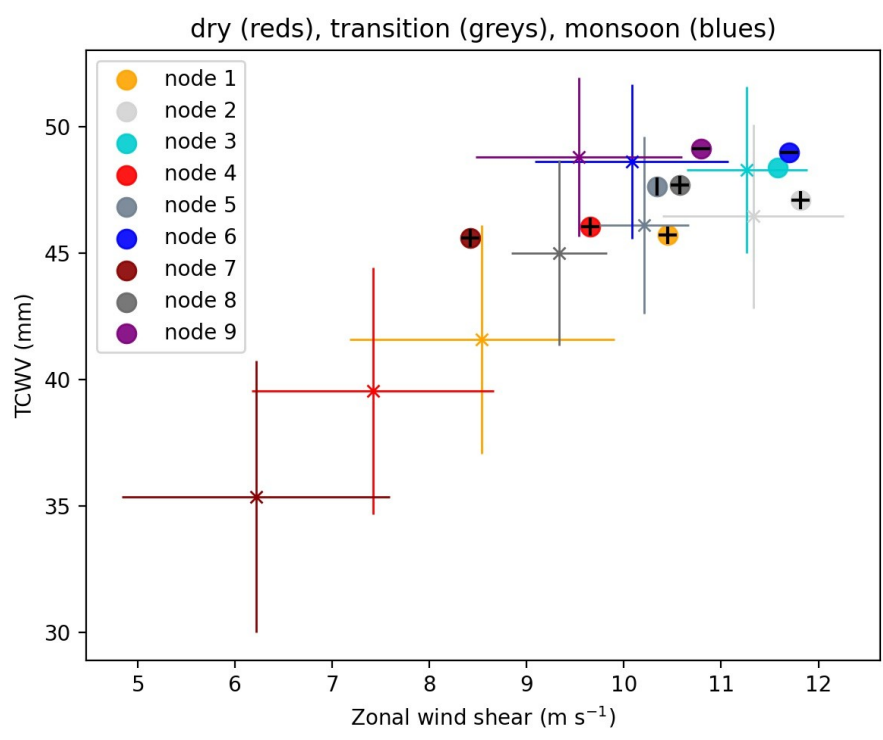
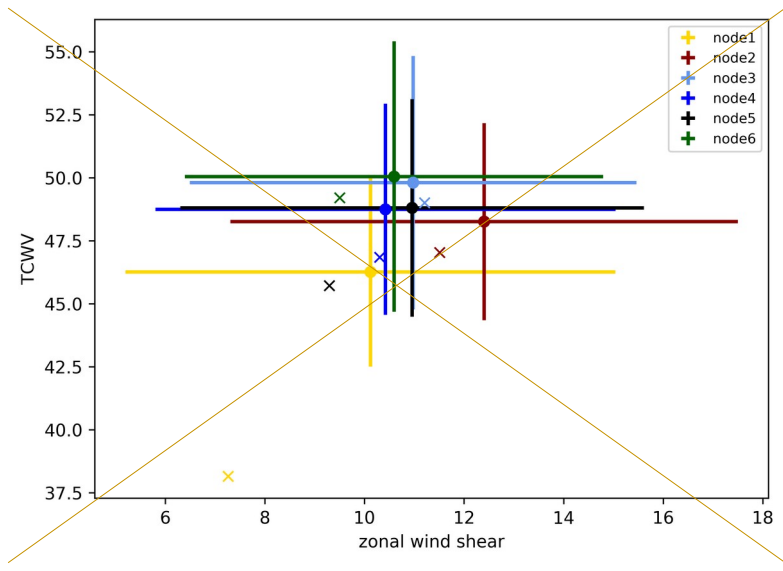
455

456 4.3 MCS driver variability within nodes

457 The drivers of MCSs within different nodes are considered to examine their relative importance within the different
 458 large-scale states (Fig. 103), concentrating on total column water vapor (TCWV) and zonal wind shear. TCWV
 459 instead of single-level specific humidity is used here to capture the changes in total moisture available to MCSs
 460 under the different regimes. For this analysis, both atmospheric drivers were sampled locally under pre-convective
 461 conditions at 1200 UTC at the location where MCSs occurred subsequently at 1800 UTC. Node 1 climatological
 462 conditions depict both, very low initial zonal wind shear and TCWV. Dry season nodes (1,4,7) exhibit the lowest
 463 climatological conditions in both wind shear and TCWV. This illustrates the relatively low storm conditions during
 464 mean conditions hostile conditions for storms in the mean for these nodes, predominantly representing dry season
 465 conditions and explaining the low storm frequency of only 0.1-1.7 MCSs per day (cf. Fig. 69). Interestingly, on
 466 storm days, conditions for this node shift to within All monsoon nodes (3,6,9) show on average slightly higher
 467 TCWV than transition nodes (2,5,8), but covering a similar range of shear conditions. Considering MCS day
 468 conditions, most nodes feature significantly higher TCWV and shear conditions relative to the climatological mean

469 node states. Solely for monsoon season nodes (3,6,9), TCWV shows no significant change, while shear still
 470 increases for nodes 6 and 9. Interestingly, for MCS days, dry season node conditions even move into the ranges of
 471 environmentclimatological conditions identified for other nodes with higher storm frequencies, albeit node 6 MCS-
 472 day conditions still represent transition season nodes, though still exhibit the lowest values in TCWV and zonal wind
 473 shear compared to MCS day conditions of transition and monsoon season nodes.

474
475
476
477
478
479
480
481
482
483
484
485
486
487
488
489
490
491
492
493
494
495
496
497
498
499
500
501
502
503
504



505 **Figure 103.** Mean MCS conditions over SWA for the different nodes. Dots show the mean within 1 standard
506 deviation (whiskers) across each node. The symbol (x) denotes the mean environmental condition for all node days
507 (MCS and non-MCS). node climatologies and MCS-day conditions over SWA. The node climatologies are depicted
508 as (x) with whiskers extending one standard deviation. Circles denote corresponding mean MCS-day conditions.
509 Horizontal black lines in the circles indicate significant differences in the shear mean, while a vertical black line
510 marks a significant difference in the TCWV mean against node climatologies based on Welch's t-tests ($p < 0.05$)

511

512 Pre-monsoon nodes (nodes 2 and 3) observe initial higher zonal wind shear conditions than all other nodes
513 with appreciably higher TCWV. Node 2 observes an increase in zonal wind shear (about 1 m/s) and also a bit more
514 TCWV. Not much change is observed in the zonal wind shear and TCWV value for node 3, making node 2 the
515 season with relatively strong instability. Comparing nodes 4 and 5 (both post-monsoon nodes), it can be observed
516 that node 5 has lower zonal wind shear to start with and thus needs higher zonal wind shear change to produce MCS
517 conditions very similar to node 4. Node 4 on the other hand shows mostly TCWV change but has a bit more zonal
518 wind shear so, in spite of the smaller zonal wind shear anomaly (Fig. 7), the resulting MCS conditions are rather
519 similar. Node 6 depicts an initial environmental condition of high TCWV over SWA, which is typical of periods
520 with frequent convective activities during peak monsoon. During MCS events, there is a slight increase in zonal
521 wind shear (about 1 m/s) and TCWV (about 0.8 kg/m^3), depicting more convective activities during the monsoon
522 season.

523 Generally, it can be noted that all nodes show increased TCWV on MCS days compared to their
524 climatology. The smallest changes for both TCWV and zonal wind shear between climatology and MCS day occur
525 for node 3, which ~~has its~~ shows the highest frequency for pre-monsoon transition month May but is still common
526 throughout the monsoon season (c.f. Fig. 1). Together with node 4, it is also the only node for which zonal wind
527 shear conditions remain approximately similar, but with climatological zonal wind shear strengths already reaching
528 $> 100 \text{ m/s}$ at MCS location. Overall, mean node environmental conditions become more similar for MCS-days
529 relative to the climatologies, illustrating that favourable MCS conditions converge towards high TCWV (~~affecting~~
530 ~~CAPE~~), and high zonal wind shear environments irrespective of the large-scale situation.

531 5 Conclusion

532 ~~The~~In this study, we identified ~~ninesix~~ synoptic states over West Africa and ~~then~~ examined what changes
533 are associated with favourable MCS environments in Southern West Africa under these states. For the definition of
534 synoptic states and MCS days, we used self-organizing maps (SOM) based on ERA5 925 hPa geopotential height
535 data and 12 years of ~~tracked~~ MCSs imagery using Meteosat Second Generation (MSG) $10.8 \mu\text{m}$ -band brightness
536 temperature data (2004-15), respectively. To investigate how the distinct synoptic states change to support MCS
537 development in SWA, we compared mean climatological node states to node sub-samples of MCS days in SWA.
538 We found the identified synoptic states, based on a 3x3 SOM matrix, to exhibit frequency distributions that are
539 linked to different phases of the West African seasonal rainfall cycle, which we classified as dry (nodes 1, 4, 7),
540 transition (nodes 2, 5, 8) and monsoon (nodes 3, 6, 9) season, albeit most nodes are not strictly confined to one

541 season. We found that different nodes identified within one season exhibit key differences in persistence
542 (consecutive node days) and node succession. Specifically, each season (dry, transition, monsoon) contains a node
543 that is frequently preceded or followed by a node of another season (nodes 1, 2, 3), as well as a node that
544 predominantly shows within-season succession (nodes 7, 8, 9). The shortest node persistence of 1.7-1.9 days was
545 found for nodes 4, 5, and 6. These nodes at the same time represent intermediate synoptic states that develop from or
546 into a different node of the same season. The SOM methodology thus seems a promising approach to identify states
547 of variability beyond the established West African monsoon phases (e.g. Thorncroft et al 2011).

548 _____ In spite of these clear differences in node persistence and succession, large-scale differences in node
549 climatologies of atmospheric MCS drivers (low-level wind field, 925hPa humidity, and temperature, CAPE) are
550 most pronounced between nodes of different seasons, while same-season nodes show strong pattern similarities.
551 Notably, however, MCS-day node anomalies, as compared to full node climatologies, all show clear increases in
552 low-level humidity and/or wind shear over the SWA region, which are important ingredients for MCS development
553 (Klein et al. 2021). For dry season nodes, these changes are associated with higher temperatures in the Sahel and
554 Sahara, driving stronger south-westerly humid winds inland while increasing shear due to an enhanced meridional
555 temperature gradient on land. Monsoon season nodes on the other hand show the opposite, where a weakening of the
556 south-westerlies and of the Sahelian low-level westerly jet indicates a south-ward shift of the monsoon circulation.
557 This results in more moisture, and for nodes 6, 9 also in higher shear, over SWA, where the latter is linked to a
558 warmer and presumably drier Sahel during monsoonal southward shifts, creating a dipole pattern. Generally, we find
559 the strongest MCS-day zonal wind shear anomalies over SWA for nodes with the strongest low-level temperature
560 anomalies to the north of SWA, representative of favorable MCS conditions in SWA during periods of a warmer
561 Sahel. Strengthened wind shear due to a warmer Sahara was previously also identified to drive MCS intensification
562 in the Sahel (Taylor et al. 2017).

563 _____ Thus, meridional displacements of the extent to which south-westerly winds from the Atlantic penetrate
564 inland and the associated positioning of the meridional temperature gradient seems to be key mechanisms by which
565 MCS days in SWA are created for both, dry and monsoon season node synoptic states. Such meridional
566 displacements have previously been identified as important drivers of monsoon variability on inter-annual (e.g.
567 Nicholson and Webster 2008) and intra-seasonal (e.g. Janicot et al. 2011, Talib et al. 2022) timescales. Here, we are
568 looking at higher-frequency changes with average node persistence between 1.7-4.3 days. Transition nodes show
569 weaker signals and a mixture of a southward (node 5) or northward (node 8) displaced circulation, which may be
570 linked to the fact that these nodes predominantly occur in months when the monsoon circulation and its rainfall band
571 are positioned over SWA (Maranan et al. 2018). Indeed, we find MCSs to be most likely to develop under transition
572 season node conditions (2.8 MCS/day across SWA domain). There is strong potential for further exploration of the
573 synoptic differences between transition season nodes and their meridional shifts on MCS days, as these may in some
574 cases be representative of monsoon onset conditions or a delayed monsoon retreat.

575 _____ Pre-convective atmospheric anomalies at locations where afternoon development of MCSs took place were
576 found to be weakest for transition season node 5, lacking significant changes in wind shear, and for monsoon season
577 nodes 3, 6, 9, for which none showed significant changes in total column moisture, albeit increased moisture at low-

578 levels contributes to elevated CAPE. Here it should be noted that weak anomalies signify nodes whose mean
579 climatological conditions already tend to be more favorable for MCS development with respect to that variable, such
580 that MCS days differ little from the node mean, which, perhaps expectedly, is the case for certain transition and
581 monsoon rather than dry season nodes.

582 Generally, however, we find node environmental conditions to become more similar for MCS days relative
583 to their node climatologies, illustrating that favorable MCS conditions converge towards high TCWV/high zonal
584 wind shear states. Overall, our results show that MCSs develop on average in high moisture, high zonal wind shear
585 local environments under all large-scale situations throughout the year. The large-scale situation however defines the
586 frequency at which favorable MCS environments can occur.~~The identified synoptic states based on the SOM nodes~~
587 ~~are noted to generally represent patterns of the seasonal rainfall cycle. Circulation patterns in node 1 can be~~
588 ~~attributed to eases primarily observed in the dry season months (January, February, November, and December). An~~
589 ~~environment representative of the pre-monsoon season is depicted by nodes 2 and 3, with node 2 presenting a clearer~~
590 ~~seasonal exclusivity. Patterns of the post-monsoon season are observed in nodes 4 and 5 with node 4 evidently~~
591 ~~depicting transition patterns that have frequent occurrences in both pre and post-monsoon seasons although~~
592 ~~prominent in the post-monsoon season. Peak monsoon conditions are clearly represented in node 6 with large-scale~~
593 ~~conditions occurring mainly in June, July, and August. The south-westerly winds observed over SWA are~~
594 ~~strengthened and move inland, enhancing moisture flow from the South Atlantic towards the land during the peak~~
595 ~~monsoon. In the pre-monsoon and post-monsoon seasons, similar but weakened south-westerly circulation patterns~~
596 ~~are observed. The synoptic-state-related MCSs realize a pronounced annual cycle of MCS numbers with frequency~~
597 ~~peaks in June and September. These peak months are well associated with maximum rainfall during the major and~~
598 ~~minor rainy seasons across SWA respectively. During the course of the year, MCSs are most likely to develop under~~
599 ~~post-monsoon conditions featuring a northward-displaced moisture anomaly (0.42 MCSs per day) which is~~
600 ~~associated with strengthened low-level westerlies, and in some cases may be representative of a delayed monsoon~~
601 ~~retreat. Furthermore, the strongest zonal wind shear anomalies over SWA are realized in seasons with the strongest~~
602 ~~low-level temperature anomalies to the north of SWA, representative of favourable MCS conditions in SWA during~~
603 ~~periods of a warmer Sahel. Regions over SWA that show stronger zonal wind shear on MCS days also depict higher~~
604 ~~CAPE. We found node environmental conditions to become more similar for MCS days relative to the node~~
605 ~~climatologies, illustrating that favourable MCS conditions converge towards high TCWV/high zonal wind shear~~
606 ~~states. Overall, our results show that MCSs develop on average in similar high moisture, high zonal wind shear local~~
607 ~~environments under all large-scale situations throughout the year. The latter however defines the frequency at which~~
608 ~~favourable MCS environments can occur.~~

609

610 *Code and data availability.* Codes for the findings of this study are available upon reasonable request from the
611 authors. The processing of ERA5 data made direct access to the primary data archive held at ECMWF, and is
612 available from the Copernicus Data Store (<https://cds.climate.copernicus.eu/>) and the MSG data are available from
613 <http://www.eumetsat.int>.

614

615 *Author contributions.* FN, NABK and CK conceptualized the study, with input from KAQ; All authors contributed
616 to and discussed the methodological design, and analyses were conducted by FN and CK; FN, ROB and KAQ wrote
617 the manuscript draft; CK, NABK, PE, GMLDQ and HAK reviewed and edited the manuscript.

618

619 *Competing interests.* The contact author has declared that none of the authors has any competing interests.

620 *Acknowledgments.* This work is supported by a grant from the Government of Canada, provided through Global
621 Affairs Canada, www.international.gc.ca (accessed on 1 January 2021), and the International Development Research
622 Centre, www.idrc.ca, (accessed on 1 June 2022) to the African Institute for Mathematical Sciences—Next Einstein
623 Initiative (AIMS-NEI) [Number: 108246-001]. CK acknowledges funding from the NERC-funded LMCS project
624 (NE/W001888/1). KQ also acknowledges funding from the National Research Foundation (NRF), South Africa.

625 **References**

626 Alfaro, D. A.: Low-Tropospheric Shear in the Structure of Squall Lines: Impacts on Latent Heating under Layer-
627 Lifting Ascent, *J Atmos Sci.*, 74, 229–48, <https://doi.org/10.1175/JAS-D-16-0168.1>, 2017.

628 Augustin, D., Pascal, I.M., Jores, T.K., Elisabeth, F.D., Cesar, M.B., Michael, T.F., Roméo-Ledoux, D.T.,
629 Marceline, M., Gladys, K.N.F. and Firmin, B.A.: Impact Assessment of the West African Monsoon on
630 Convective Precipitations over the Far North Region of Cameroon, *Adv. Space Res.*,
631 <https://doi.org/10.1016/j.asr.2022.04.044>, 2022.

632 Baidu, M., Schwendike, J., Marsham, J.H. and Bain, C.: Effects of Vertical Wind Shear on Intensities of Mesoscale
633 Convective Systems over West and Central Africa, *Atmos. Sci. Lett.*, e1094, <https://doi.org/10.1002/asl.1094>,
634 2022.

635 Biasutti, M., Sobel, A. H., & Camargo, S. J.: The role of the Sahara low in summertime Sahel rainfall variability and
636 change in the CMIP3 models. *Journal of Climate*, 22(21), 5755-5771,
637 <https://doi.org/10.1175/2009JCLI2969.1>, 2009.

638 Cassano, E.N., Glisan, J.M., Cassano, J.J., Gutowski Jr, W.J. and Seefeldt, M.W.: Self-Organizing Map Analysis of
639 Widespread Temperature Extremes in Alaska and Canada, *Clim. Res.* 62, 199-218,
640 <https://doi.org/10.3354/cr01274>, 2015.

641 Chen, Y., Luo, Y. and Liu, B.: General Features and Synoptic-Scale Environments of Mesoscale Convective
642 Systems over South China during the 2013-2017 Pre-Summer Rainy Seasons, *Atmos. Res.*, 266,
643 <https://doi.org/10.1016/j.atmosres.2021.105954>, 2022.

644 Feng, Z., Leung, L.R., Liu, N., Wang, J., Houze Jr, R.A., Li, J., Hardin, J.C., Chen, D. and Guo, J. A.: Global High-
645 Resolution Mesoscale Convective System Database Using Satellite-Derived Cloud Tops, Surface
646 Precipitation, and Tracking, *J. Geophys. Res. Atmos.* 126, e2020JD034202,
647 <https://doi.org/10.1029/2020JD034202>, 2021.

648 Guo, Y., Du, Y., Lu, R., Feng, X., Li, J., Zhang, Y. and Mai, Z.: The Characteristics of Mesoscale Convective
649 Systems Generated over the Yunnan-Guizhou Plateau during the Warm Seasons, *Int. J. Climatol.*,
650 <http://doi.org/10.1002/joc.7647>, 2022.

- 651 Guy, N., Rutledge, S.A. and Cifelli, R.: “Radar Characteristics of Continental, Coastal, and Maritime Convection
652 Observed during AMMA/NAMMA”, Q. J. R. Meteorol. Soc. 137, 1241-56, <http://doi.org/10.1002/qj.839>,
653 2011.
- 654 [Hagos, S. M. and Cook, K. H.: Dynamics of the West African Monsoon Jump, J. Clim., 20\(21\), 5264–5284,
655 <https://doi.org/10.1175/2007JCLI1533.1>, 2007.](https://doi.org/10.1175/2007JCLI1533.1)
- 656 Hewitson, B. C., & Crane, R. G.: Climate Downscaling: Techniques and Application. Clim. Res. 7, 85-95,
657 <https://doi.org/10.3354/cr007085>, 1996.
- 658 Hewitson, B. C., & Crane, R. G. “Self-Organizing Maps: Applications to Synoptic Climatology.” Clim. Res. 22, 13-
659 26, <https://doi.org/10.3354/cr022013>, 2002.
- 660 Hodges, K.I. and Thorncroft, C.D.: Distribution and Statistics of African Mesoscale Convective Weather Systems
661 Based on the ISCCP Meteosat Imagery, Mon Weather Rev 125, 2821-37, [https://doi.org/10.1175/1520-
662 0493\(1997\)125<2821:DASOAM>2.0.CO;2](https://doi.org/10.1175/1520-0493(1997)125<2821:DASOAM>2.0.CO;2), 1997.
- 663 Houze Jr, Robert A.: Mesoscale Convective Systems”, Rev. Geophys., 42, <http://doi.org/10.1029/2004RG000150>,
664 2004.
- 665 Hussain, M.S., Kim, S. and Lee, S.: On the Relationship between Indian Ocean Dipole Events and the Precipitation
666 of Pakistan, Theor. Appl. Climatol. 130, 673-85, <http://doi.org/10.1007/s00704-016-1902-y>, 2017.
- 667 IPCC: Climate Change, 2014: Synthesis Report. Contribution of Working groups I, II, and III to the Fifth
668 Assessment Report of the Intergovernmental Panel on Climate Change [Core Working Team, R.K. Pachauri
669 and L.A. Meyer (eds)]. IPCC, Geneva, Switzerland, 151, 2014
- 670 [Janicot, S., Caniaux, G., Chauvin, F., De Coëtlogon, G., Fontaine, B., Hall, N., Kiladis, G., Lafore, J.-P., Lavaysse,
671 C., Lavender, S.L., Leroux, S., Marteau, R., Mounier, F., Philippon, N., Roehrig, R., Sultan, B. and Taylor,
672 C.M.: Intraseasonal variability of the West African monsoon. Atmospheric Science Letters, 12, 58–66.
673 <https://doi.org/10.1002/asl.280>, 2011](https://doi.org/10.1002/asl.280)
- 674 Janiga, M.A. and Thorncroft, C.D.: The Influence of African Easterly Waves on Convection over Tropical Africa
675 and the East Atlantic, Mon Weather Rev 144, 171-92, <https://doi.org/10.1175/MWR-D-14-00419.1>, 2016.
- 676 Kamara, S. I.: The Origins and Types of Rainfall in West Africa, Weather 41, 48-56, [https://doi.org/10.1002/j.1477-
677 8696.1986.tb03787.x](https://doi.org/10.1002/j.1477-8696.1986.tb03787.x), 1986.
- 678 Kim, H.K. and Seo, K.H.: Cluster Analysis of Tropical Cyclone Tracks over the Western North Pacific Using a Self-
679 Organizing Map, JCLI 29, 3731-51, <https://doi.org/10.1175/JCLI-D-15-0380.1>, 2016.
- 680 Klein, C., Belušić, D., & Taylor, C. M.: Wavelet scale analysis of mesoscale convective systems for detecting deep
681 convection from infrared imagery. Journal of Geophysical Research: Atmospheres, 123, 3035 - 3050.
682 <https://doi.org/10.1002/2017JD027432>, 2018.
- 683 Klein, C., Nkrumah, F., Taylor, C.M. and Adefisan, E.A.: Seasonality and Trends of Drivers of Mesoscale
684 Convective Systems in Southern West Africa, JCLI 34, 71-87, <https://doi.org/10.1175/JCLI-D-20-0194.1>,
685 2021.
- 686 Kohonen, T. “Self-Organizing Maps.-Springer Series in Information Sciences, V. 30, Springer Sci. Rev.,
687 <https://doi.org/10.1007/978-3-642-56927-2>, 2001.

- 688 Kusangaya, S., Warburton, M.L., Van Garderen, E.A. and Jewitt, G.P.: Impacts of Climate Change on Water
689 Resources in Southern Africa: A Review, *Phys. Chem. Earth.*, 47-54,
690 <https://doi.org/10.1016/j.pce.2013.09.014>, 2014.
- 691 Laing, A.G., Carbone, R., Levizzani, V. and Tuttle, J.: The Propagation and Diurnal Cycles of Deep Convection in
692 Northern Tropical Africa, *Q J R Meteorol Soc.* 134, 93-109, <http://doi.org/10.1002/qj.194>, 2008.
- 693 Lavaysse, C., Flamant, C., Janicot, S., Parker, D.J., Lafore, J.P., Sultan, B. and Pelon, J.: Seasonal Evolution of the
694 West African Heat Low: A Climatological Perspective, *Clim. Dyn.* 33, 313-30,
695 <https://doi.org/10.1007/s00382-009-0553-4>, 2009.
- 696 Le Barbé, L., Lebel, T., & Tapsoba, D.: Rainfall variability in West Africa during the years 1950 - 90. *J. Clim.*
697 15(2), 187-202, [https://doi.org/10.1175/1520-0442\(2002\)015<0187:RVIWAD>2.0.CO;2](https://doi.org/10.1175/1520-0442(2002)015<0187:RVIWAD>2.0.CO;2), 2002.
- 698 Li, P., Moseley, C., Prein, A.F., Chen, H., Li, J., Furtado, K. and Zhou, T.: Mesoscale Convective System
699 Precipitation Characteristics over East Asia. Part I: Regional Differences and Seasonal Variations, *J. Clim.*
700 33, 9271-86, <https://doi.org/10.1175/JCLI-D-20-0072.1>, 2020.
- 701 Maranan, M., Fink, A.H. and Knippertz, P.: Rainfall Types over Southern West Africa: Objective Identification,
702 Climatology and Synoptic Environment, *Q J R Meteorol Soc.* 144, 1628-48, <https://doi.org/10.1002/qj.3345>,
703 2018.
- 704 Mohr, K. I., and Zipser, E. J.: Mesoscale convective systems defined by their 85-GHz ice scattering signature: Size
705 and intensity comparison over tropical oceans and continents. *Mon. Wea. Rev.*, 124, 2417-2437,
706 [https://doi.org/10.1175/1520-0493\(1996\)124<2417:MCSDBT>2.0.CO;2](https://doi.org/10.1175/1520-0493(1996)124<2417:MCSDBT>2.0.CO;2), 1996
- 707 Mohr, K.I. and Thorncroft, C.D.: Intense Convective Systems in West Africa and Their Relationship to the African
708 Easterly Jet, *Q J R Meteorol Soc.* 132, 163-76, <https://doi.org/10.1256/qj.05.55>, 2006.
- 709 Nesbitt, S.W., Cifelli, R. and Rutledge, S.A.: Storm Morphology and Rainfall Characteristics of TRMM
710 Precipitation Features, *Mon Weather Rev* 134, 2702-21, <https://doi.org/10.1175/MWR3200.1>, 2006.
- 711 [Nicholson, S. E. and Webster, P. J.: A physical basis for the interannual variability of rainfall in the Sahel, *Q. J. R. Meteorol. Soc.*, 2084 \(November\), 2065–2084, doi:10.1002/qj. 2008.](#)
712
- 713 Queralt, S., Hernández, E., Barriopedro, D., Gallego, D., Ribera, P. and Casanova, C.: North Atlantic Oscillation
714 Influence and Weather Types Associated with Winter Total and Extreme Precipitation Events in Spain,
715 *Atmos. Res.* 94, 675-83, <https://doi.org/10.1016/j.atmosres.2009.09.005>, 2009.
- 716 Schmetz, J., Pili, P., Tjemkes, S., Just, D., Kerkmann, J., Rota, S. and Ratier, A.: An Introduction to Meteosat
717 Second Generation (MSG)", *Bull Am Meteorol Soc* 83, 977-92, [https://doi.org/10.1175/1520-0477\(2002\)083<0977:AITMSG>2.3.CO;2](https://doi.org/10.1175/1520-0477(2002)083<0977:AITMSG>2.3.CO;2), 2002.
- 719 Schrage, J.M., Fink, A.H., Ermert, V. and Ahlonsou, E.D.: Three MCS Cases Occurring in Different Synoptic
720 Environments in the Sub-Sahelian Wet Zone during the 2002 West African Monsoon, *J Atmos Sci* 63, 2369-
721 82, <https://doi.org/10.1175/JAS3757.1>, 2006.
- 722 Sheridan, S. and Lee, C.C.: Synoptic Climatology and the Analysis of Atmospheric Teleconnections, *Prog Phys*
723 *Geogr.* 36, 548-57, <https://doi.org/10.1177/0309133312447935>, 2012.
- 724 Sultan, B., & Janicot, S.: The West African monsoon dynamics. Part II: The “preonset” and “onset” of the summer
725 monsoon. *Journal of climate*, 16(21), 3407-3427, [https://doi.org/10.1175/1520-0442\(2003\)016<3407:TWAMDP>2.0.CO;2](https://doi.org/10.1175/1520-0442(2003)016<3407:TWAMDP>2.0.CO;2), 2003.

- 727 | [Talib, J., Taylor, C. M., Klein, C., Harris, B. L., Anderson, S. R. and Semeena, V. S.: The sensitivity of the West](#)
728 | [African monsoon circulation to intraseasonal soil moisture feedbacks, Q. J. R. Meteorol. Soc., 148\(745\),](#)
729 | [1709–1730, doi:10.1002/qj.4274, 2022.](#)
- 730 | Taylor, C.M., Belušić, D., Guichard, F., Parker, D.J., Vischel, T., Bock, O., Harris, P.P., Janicot, S., Klein, C. and
731 | Panthou, G.: Frequency of Extreme Sahelian Storms Tripled since 1982 in Satellite Observations, Nature 544,
732 | 475-78, <https://doi.org/10.1038/nature22069>, 2017.
- 733 | [Thorncroft, C. D., Nguyen, H., Zhang, C. and Peyrille, P.: Annual cycle of the West African monsoon: Regional](#)
734 | [circulations and associated water vapour transport, Q. J. R. Meteorol. Soc., 137\(654\), 129–147,](#)
735 | <https://doi:10.1002/qj.728>, 2011.
- 736 | [Thorncroft, Chris D., Hanh Nguyen, Chidong Zhang, and Philippe Peyrille.: Annual Cycle of the West African](#)
737 | [Monsoon: Regional Circulations and Associated Water Vapour Transport, Q. J. R. Meteorol. Soc. 137, 129-](#)
738 | [47, https://doi.org/10.1002/qj.728](https://doi.org/10.1002/qj.728), 2011.
- 739 | Vizzy, E.K. and Cook, K.H.: Mesoscale Convective Systems and Nocturnal Rainfall over the West African Sahel:
740 | Role of the Inter-Tropical Front, Clim. Dyn. 50, 587-614, <https://doi.org/10.1007/s00382-009-0553-4>, 2018.
- 741 | Wolski, P., Jack, C., Tadross, M., van Aardenne, L. and Lennard, C.: Interannual Rainfall Variability and SOM-
742 | Based Circulation Classification”, Clim. Dyn. 50, 479-92, <https://doi.org/10.1007/s00382-017-3621-1>, 2018.
743